Author response by Tom Jordan on behalf of all other authors, June 2018

First, we would like to thank both reviewers for their constructive and thoughtful reviews and the editorial team for handling our submission. We have been able to fully address the suggested changes and we think that our manuscript is improved from the previous submission. Our responses and actions are in blue text.

Review 1

General Impression:

Jordan et al. analyze an extensive radar dataset covering large parts of Greenland. They introduce a novel metric ("the bed reflectivity variability") to locate basal water at the ice-bed interface. This is potentially a sufficient (but not a necessary) condition for water at the ice sheet base. The results can, for example, be used as a constraint for modelling the evolution of the Greenland Ice Sheet, which critically depends on the conditions at the basal boundary (wet vs. dry).

I have read this paper with great interest, and the authors do an excellent job in guiding the reader through the manuscript. Basic methodology is explained succinctly (incl. appropriate references), and novel parts are correspondingly highlighted and more detailed. All Figures are informative and of high quality. I am impressed with the scope of the analysis, which includes a very rich radar dataset, and the careful interpretation of the "basal reflectivity variability" as a new (but not the only) metric for basal water. In the following, I have a number of comments which should be addressed, and which hopefully will make the paper stronger. I believe that this paper will be useful for other researchers in the future, and apologize to the authors, and to the editor, for the delayed submission of this review.

Kind regards,
Reinhard Drews, Geosciences, University of Tübingen, Germany

Thanks – this is a really tight summary of both the purpose and results of our study.

Interpretation of basal reflectivity variability

The authors make it clear (in l. 368) that reflectivity variability above the chosen threshold is a sufficient criterion for basal water. However, the converse argument (that is: low reflectivity variability, hence, absence of basal water) does not hold. It is very important that people using the results of this study are aware of this, and it should be mentioned more clearly (i.e. in the abstract and elsewhere). The importance of this point is highlighted because the authors themselves misinterpret their own results in this regard. The inference that "…basal water is often concentrated in the fast-flow onset regions and tributaries whilst it is ***absent*** from the main trunk." (l. 457) is not valid, because the absence of elevated bed reflectivity does not necessitate the absence of basal water (it could simply be homogenously distributed and thus not be visible with this metric). I see much potential for misinterpretation here, and the authors should describe the limitations of this novel metric in a more pronounced way.

We agree - it is vital that our basal water criterion is interpreted correctly (particularly by non-radioglaciology specialists who may be interested in the results but not the fine details). In light of this comment we have made the following changes:

(i) We have been upfront in 4 key sections (abstract, final paragraph of intro, intro to results, conclusion) that the RES diagnostic is a `sufficient but not necessary' criteria for basal water.
(ii) We have change title of section 2.5 to: *Interpretation of reflectivity variability as a sufficient diagnostic for basal water*
(iii) We have deleted the section related to L 457, where we (likely mistakenly) interpret the absence of basal water.
(iv) In Sect. 4.6 we now cross-reference the basal reflectivity/water map in Chu et al. 2018. This provides further support to our assertion that water diagnostic is well tuned to capture finite water bodes in the interior/fast flow initiation region of Petermann but will not capture homogeneously reflective wet sediment in the main trunk.

2. Derivation of basal reflectivity variability:

Does it matter that only log-transformed variables are used? I wonder this, because:

$$VAR\ 10\ log10(X) \neq 10log10\ VAR\ X$$

I can see the convenience of the log-transform when interpreting the reflection amplitudes, but I am unsure if this causes problems when calculating variances (and variance of multiplicative variables). Is there an underlying assumption about the statistics/uncertainties that was not explicitly mentioned? I understand this is a somewhat diffuse comment.

This is a helpful comment. See our related response to reviewer 2.

3.Crossing-Over Analysis of the bed reflectivity variability

The authors should do a crossing-over analysis of the bed reflectivity variability. This would strengthen the argument that birefringence and radar system specifics are small. It will also more clearly demonstrate the robustness of the new metric and highlight its advantages (which is that radar data collected over multiple field seasons and with various radar systems can efficiently be combined).

We have added an Appendix A demonstrating cross-over statistics using MCoRDS v2 (the most recent and spatially extensive set of measurements) as a baseline.

When interpreting this analysis, it is important to note that the cross-over standard deviations for sigma_[R] are not necessarily to be interpreted as standard errors. This is because the flight-track windows that are compared, do not sample the same region of the glacier bed (and are likely significant overestimates). This contrasts with performing cross-over analysis of bed-echo power/reflectivity where the Fresnel zone defines a spatial overlap. As a form of edge detector, the purpose of the sigma_[R]

metric is to identify a signal attributable to basal water within a 5 km region (rather than to coarse-grain an average value at the window size). Additionally, the along-track data in Fig. 2 shows that sigma_[R] can rapidly fluctuate at a 5 km length scale. We therefore point toward the high degree of spatial structure in the water predictions (including intersecting flight lines from multiple years) as evidence for the robustness of the approach.

4. Discrimination between water patches and smooth--rough transitions

Variability in bed roughness is a competing mechanism which would also result in elevated bed-reflectivity variability. The authors are aware of this and suggest that the threshold is well tuned to discriminate between these two scenarios. However, I did not fully understand why this is the case and the manuscript is in this regard unfortunately too vague (e.g. "..we demonstrate later …" (l. 309) but where is this actually done?). This is important, because interpretation of the "bed reflectivity variability" as a proxy for basal water is a central conclusion of this paper, and other options must be convincingly excluded.

We agree with the reviewer that we need to be clearer on this point. In previous work, Jordan et al. 2017, we surveyed radar bed-roughness in northern Greenland (using both topographic-scale roughness, and the bed-echo abruptness/peakiness as a proxy for radar wavelength scale roughness). A visual comparison between the water map in this study and the roughness maps in Jordan et al. 2017, demonstrates that the water hits can occur in both smooth and rough regions of the bed. Moreover, comparison with ice-sheet scale spectral analysis of roughness by Rippin 2013, also demonstrates that both relatively rough and smooth regions can have water present (at least the length-scale considered).

In summary, we therefore think that the water diagnostic is not significantly modulated by spatial patterns in bed roughness, and is therefore is well tuned for ice-sheet scale analysis (by contrast, the previous water detection method used in Greenland by Oswald and Goginneni 2008, 2012 will only work in spatially-extended smooth regions where there are peaky waveforms).

We now realise that this is better incorporated in the discussion so have:

(i) removed L. 309 from the methods.

(ii) In sect 4.5 been more explicit about the lack of apparent modulation by roughness of our water map.

Additionally, we also now note in Sect 2.5 that whilst roughness (specular/diffuse scattering) transitions likely correlate with wet-dry transitions, this will actually act to amplify the signal component we are interested in (high values of sigma_[R])

Finally, cross-over analysis of sigma_[R] for the lower frequency (150 MHz) radar systems against the 195 MHz (Mcords v2) benchmark, does not show a significant bias (see the new Appendix A). This is further supporting evidence for (lack of) power modulation due to roughness and the assumptions made in the extraction of bed echo power (i.e. we aimed to suppress roughness-induced variability by integrating bed-echo power in fast time over the echo envelope). This has been added to 2.5.

5. Temperature profile near ice divides

I disagree that in the interior of ice sheets GHF and vertical diffusion are the dominant processes. What about vertical advection? In Greenland the surface mass balance is significant in the interior and thus I would expect a (strongly) non-linear temperature profile with depth (which would not be the case if only diffusion was important). A quick-look at the NGRIP profile does confirm this. Can you comment on this?

We agree with the reviewer. We have now added `and vertical advection' to line 393.

6. Attenuation correction using modelled temperatures

Briefly explain what the modelled temperature field of Goelzer et al., 2013 is based on, (how it compares to in-situ measurements), and how it may impact your results. Is it possible that temperature variations near the coast (where ice streaming is significant) are smoothed out, and thus do not correctly cancel the attenuation in your approach?

We have now added the following text about the temperature field to Sect. 2.2

The temperature field derives from a full 3D thermomechanical simulation over several glacial-interglacial cycles and is subsequently rescaled to a 1 km representation of the Bamber et al. 2013 ice thickness data set. The geothermal heat flux in GISM was initially taken from Shapiro and Ritzwoller 2004, but further adjusted with Gaussian functions around the deep ice core sites to match observed basal temperatures. Vertical temperature profiles are within 1-2 degrees C when compared to available in-situ measurements. GISM resolves the flow on a model resolution of 5 km, which causes some smoothing of the temperature field in narrow outlet glaciers near to the coast.

We therefore agree that the horizontal resolution of the temperature/attenuation field is coarser than some of the narrow flow features around the ice-sheet margins. However, our `sensitivity/perturbation analysis' in Sect 2.6 does provides a way to assess sources of bias in the attenuation model (including temperature). Note; we take a conservative approach of eliminating water-hits that do not satisfy the sigma_[R]>6 dB criteria when the model is perturbed.

7. Ice Fabric Variations

I agree that fabric variations are a small component in the overall backscattered power budget. However, could it be that the "corridor" along the central ice divide is to some degree linked to ice anisotropy? Across a divide, ice fabric can change abruptly (compared to your 5 km window) (e.g. Martin et al., J. Geophys. Res., 2009; Drews et al., J. Glac., 2012) and potentially this may impact the inferred "bed reflectivity variability".

This is an interesting point! We interpret this as corresponding to regions where there is a pronounced azimuthal shift in the dielectric principal axes at a scale < 5 km. However, without access to polarimetric sounding data, this is difficult to test (and, in the general case where there are no cross-overs, correct

for). Whist we acknowledge the role of power modulation due to birefringent propagation (e.g. Matsuoka et al. 2012c), we do not think that flight track orientation (which would relate to the proposed fabric mechanism) has a dominant influence/bias upon the water hits. Supporting evidence for this, is the fact that the water hits in the ice-divide regions - see zooms 7(b), 7(d), 9(d) - occur a range of flight orientations relative to the ice-divide (which should correlate with the orientation of the dielectric principle axes).

We have added this point to the discussion (Sect. 4.6) along with referencing Martin et al .2009, Drews et al. 2012 and Matsuoka et al. 2012 cfor extra context upon the impact of ice fabric.

As an aside, power modulation (or lack of) due to ice fabric is another potential reason why we believe reflectivity variability to have certain `calibration advantages' over mapping basal reflectivity (which combines reflection values from multiple orientations). This is because, if we consider the (likely more general) case where the dielectric principal axes vary negligibly in orientation over a 5 km linear window, then there will be less potential power modulation due to fabric than if one were combining measurements from multiple orientations (e.g. Fig. 7 in Matsuoka et al. 2012c, JGR).

Minor Suggestions

Maybe "A sufficient constraint upon basal water distribution beneath the Greenland Ice Sheet from radar bed echo variability" would be a better (and slightly shorter) title?

If possible, we would like to retain *`A constraint upon the basal water distribution and thermal state of the GrIS from radar bed-echoes*' as the connection with the thermal state/basal temperature is a central purpose of the MS (note -we have now dropped `basal' from basal thermal state to shorten the title) However, we have now been explicit in the abstract that our water diagnostic is interpreted as a sufficient (but not a necessary) criteria for basal water.

l. 320 There is a missing section number in the internal reference.

We have now added Sect. 2.2.

l. 580 Basal 'freeze-on' is one, but not the only explanation for the disturbances seen at larger depth. Concerns about this (e.g. Dow et al., Geophys. Res. Lett., 2018) or other explanations (e.g. Bons et al., Nat. Comms., 2016) should also be mentioned here.

A good point. We have now referred to the englacial features using the more generic term `Basal units of disrupted radiostraitigraphy' (following Dow et al. 2018) and added the additional explanations in Bons et al. 2016 (anisotropic rheology), Wolovick et al. 2014 (stick-slip mechanism).

Fig. 5b add y-label ([R] (db))

Done

Review 2

Summary: This paper uses a RES diagnostic the author's term "bed-echo reflectivity variability" for the long archive of RES observations over Greenland to get at the distribution of basal water. They then proceed to compare this to various prediction for the distribution of subglacial water. It is comprehensive and thorough, however I cant help thinking its being presented as a lot more sophisticated than it actually is. High passing radar data has been a (justifiable) refuge of radioglaciologists since the C-130 TUD days, and thats basically what seems to be happening here - just in slow time rather than fast time.

We do agree that, viewed from a technical standpoint, our radar method is (relatively) simple. However, the novelty and impact of our study is primarily due to our geographical analysis of an extensive radar data set across the ice sheet. This is the first time that an ice-sheet-wide assessment of basal water has been done with a post-2003 radar data set.

Major issues: Novelty: Bed echo variability has been long used for characterizing basal interface (Neal, 1982; Peters et al., 2005; Carter et al., 2007), and the surface interface (Grima et al., 2014) - most of this literature is not mentioned from this context. The authors here extend to very long length scales, and integrate in fast time over the echo to suppress roughness effects in an attempt to essentially map out subglacial water using an assumption of bimodal wet/dry distribution, to get around variability in attenuation that will inevitably bias absolute values.

We apologise for the previous omission of this literature, and now have included an extra paragraph to the relevant methods section (2.3) describing the prior work of Neal, Peters, Carter and Grima, clarifying the differences with our approach:

'*It is important to clarify the difference between the use of bed-echo power/reflectvity variability in this study from previous radioglaciology studies (Neal1982, Peters et al. 2005,Carter et al. 2007,Grima et al. 2014). These studies focused upon the variability/statistics of the peak echo power as a result of phase modulation by interfacial roughness. By contrast, in this study we suppress roughness effects by integrating power in fast time over the echo envelope. We are therefore able to focus upon power variability that is a result of along-track changes in the bed dielectric.'*

Edge detection: The approach I feel is misnamed. From Figure 2 it seems clear that large scale changes dominate their analysis, and thus basically what the authors have is an edge detector. What they are finding is not so much variability as gradients. In order to get at the small scale variability indicated in figure 5b, they would have to high pass the data, which they are not doing. A multi-scale approach may be more productive to get at mixed media cases.

The reviewer is correct and the approach we take can be viewed as a form of edge detection. However, the purpose of plot 5b is to show that the approach is not limited to a singular transition (i.e. the variability approach will be able detect more water hits than if a singular transition/conventional edge detector is imposed). In other words, we are not necessarily interested in detecting/classifying fine-scale variability, (we just did not want to impose that a singular dielectric transition was present).

It is important to bear in mind, that our method was tuned around the (in our view necessary requirement) of making a comparison to the basal thermal state synthesis by Macgregor et al. 2016 (this assumed a resolution of 5 km, which is also an appropriate scale for informing ice-sheet scale numerical models). This is specifically why we did not consider a multi-scale approach. Additionally, previously identified GL water bodies are small (< 5 km), so we were concerned that if we imposed a singular transition at the prescribed resolution, then we would miss a significant fraction of the basal water.

Based upon this helpful comment, we have made the following changes:

(i) In the abstract, and other key sections where we discuss bed-echo reflectivity variability we have highlighted that it acts as a form of edge detector.

(ii) We have been explicit that we used this approach (rather than other methods of edge detection) as we do not wish to limit ourselves to a singular wet-dry/dielectric transition in a 5 km window.

(iii) We now have now revised the introduction to Section 2.3, better explaining the context for the introduction of our method (particularly, motivating our choice of length-scale regarding the comparison later made with Macgregor et al. 2016).

Statistics in dB space: I am concerned at the application of statistics in dB space, and think this needs to be better motivated. Due to the compression of the distribution of the echoes using the attenuation model, and the highly bimodal reflectivity of the bed, they 'get away with it' somewhat; however, I attach an jupyter notebook that attempts to illustrate the complexities of doing the variability statistics in dB using a synthetic fractal distribution (again, the hypothesized distribution will be more bimodal, but there will be a sensitivity long wave length errors in attenuation) and a bimodal distribution.

We thank the reviewer for their detailed feedback on this subtle point and have read their jupyter notebook with interest. We have now added the qualifying statement to Sect. 2.3 that we consider the variability of the log-transformed variables (and that this differs from the variability of the linear variables in log space). However, since our 6 dB water threshold was devised with the log-transformed variables in mind, we genuinely do not think that there is an issue with our approach (and, for reasons given below, we think that are certain benefits).

Specifically, our motivation for using dB space is:

(i) That it enables a clearer connection to be made with the dB reflection amplitudes for various geophysical media (which are more familiar to the radioglaciology community than linear Fresnel values). It is also to be noted that the radioglaciology community (either implicitly or explicitly) apply reflectivity statistics in dB space regarding water detection (e.g. MacGregor et al 2013, Wolovick et al. 2013).

(ii) The log-transform enables us to consider the additive form of the radar power equation (which results in the simpler to interpret VAR([R]) +VAR([L]) rather than VAR(R*L))

These points have now been added to Sect 2.3, along with a qualifying statement in 2.6 that the 6dB threshold only applies to log-transformed reflectivity.

Calculation of sigma: It wasn't clear if you are taking the deviation in power of points separated by 5 km, or just taking the standard deviation of all points within the 5 km window.

We take the standard deviation of all points within the window. This has now been made clear in Sect 2.3.

Ice surface transmission losses: Surface losses due to roughness or near surface englacial water are not considered. I think for this paper they could be important, as they do not correlate with the predictions for whole ice sheet attenuation, and have the potential for sharp gradients. Surface and near surface losses should be addressed maybe just by a demonstration that they are negligible.

Regarding this point, it is important to bear in mind the central purpose of our study and the impact upon the central results/conclusions (specifically, the assessment of regions of basal thaw & the comparison we make with Macgregor et al. 2016 and the GHF maps). We note that regions susceptible to surface water/surface roughness-induced variability are toward the margins/faster flowing. We are therefore only likely to get `false positives' for basal water (i.e. anomalously high variability) in regions where there is a already a high degree of confidence that there is a warm thermal regime. This surface modulation therefore, does not have a large impact on the thermal state comparison (since we are primarily interested in water hits in the slow-flow regions previously predicted to be frozen), or the GHF comparison (since we limit this comparison to the interior ice divides).

In summary; whilst we do agree with the reviewer that these effects are present, we believe that there will be minor impact upon our take-home results/conclusions. However, we do agree that this should be added to the discussion and have now added an extra paragraph. And referenced Grima et al. 2014 and Schroeder et al. 2016a regarding surface roughness—induced power variability (see Sect 4.6).

Minor issues:

Data traceability: The authors need to emphases that these data are from the CSARP processor found on the KU website, and NOT the MDVR processed data found on the NSIDC website. The latter should not be used for quantitative analysis of the bed echo. NSIDC says this in their website, but a disclaimer here might help head off confusion.

In sect 2.1 & and the data availability section we have now added explicitly that we are using the CSARP data.

Along track processing: There is very little detail on how azimuth processing has changed over time, and how this could effect the results.

The new Appendix A (cross-over statistics for reflectivity variability) provides an instrument-by-instrument breakdown, demonstrating no significant/minor cross-over biases. This provides an empirical test that the data is suitable for combined interpretation.

We already give 3 references in 2.1 regarding radar signal processing (Rodriguez-Morales et al 2014, Gogineni et al 2014, Paden2015), and believe that presentation is at the correct level of detail for the (primarily glaciological) readership of TC.

Also not clear: did the author do along track incoherent averaging as they did for earlier papers?

No – this was not done. This was discussed with the CReSIS radar team, and was deemed an unnecessary (but inconsequential) step in the prior work, with the (non-averaged) L1B data product being preferable. The overall effect of the prior-averaging is to decrease the spatial resolution. However, since in Jordan et al. 2016, we chose to grid the data anyway. there are no significant consequences for the maps in the paper.

We now have added that we did not do this step to Sect 2.1.

Power determination approach: The method for extracting aggregate power, and rejecting bad echoes, appears to have changed between Jordan et al 2016, 2017. In those works, a symmetrical window about the peak is taken, while in this work, a 10 dB threshold down from the peak power is used. A 10 dB SNR is used here, while in earlier work it appears to be a 17 dB threshold is used. The change needs to be better justified, and the opportunity taken to explain if there is any impact of the results of the earlier papers.

The reviewer is correct and we have applied a less strict SNR criteria in this study (10 dB rather 17 dB). The justification for this change is that we now believe that were overly strict in the previous studies. If the old 17 dB threshold is used then there is a decrease in the effective coverage in southern Greenland.

The impact upon the previous works is that the `effective coverage' of the radar flight-track data that is analyzed will be slightly smaller than for this paper. As the previous papers were technique (rather than data set) orientated papers we do not foresee any significant issues.

Figure 2: I suggest the authors reverse the order of intensity (i.e. have sigma solid and black, and have the power a lighter line). I also suggest adding the 6 dB threshold to the second row.

If possible, we would like to keep the sigma variables in color. However, we have now increased the line thickness of the sigma variables and decreased the line thickness/intensity of the solid black lines. The 6 dB threshold has also now been added in as suggested.

Figure 8c: I think that Martos's data does need to be considered from the POV of the input magnetic track lines, especially from this sort of comparison.

First, we interpret `this sort of comparison' in relation to the different spatial scales at which the radar water predictions and GHF models are assessed at and POV to mean `point of view'. In which case, we agree that it is important to add a qualifying section on this and have added:

In the comparison between the radar water predictions and GHF in Fig. 8 it is important to bear in mind that the GHF distributions are evaluated at a lower spatial resolution. For example, the resolution of the GHF distribution by Martos et al. 2018/in revision is a consequence of the spectral method (window size and overlap) which has an effective resolution of ~ 75 km.

Martos et al. 2018/in revision, is close to being accepted for publication at GRL and we hope to reference the published work in our final paper. The question of magnetic track spacing was dealt with extensively in their review process/paper and we therefore do not think it is necessary to include any more information in our MS. However, for completeness, we now briefly summarize the key points:

- Martos et al. 2018/in revision used magnetic anomaly data from the World Digital Magnetic Anomaly Map v2 (WDMAM v2) compilation to derive Curie Depths from which the GHF is estimated.
- The WDMAM v2 is based on a good line coverage of Greenland with datasets described in the WDMAM v2 report. The provided original format of these datasets contain grid cells between 1 and 5km. The sparsest line spacing separation in this compilation in a specific part of North Greenland with 60 km between track lines. The coverage is much denser over the rest of Greenland, reaching line spacings <10 km.
- The (de-fractal) spectral method applied to the magnetic data uses window sizes of 350 km x 350 km with a 57% overlap. With the spectral method the depth to the top and the depth to the centroid of the deepest magnetic sources are identified and assigned to the central part of the window (spatial resolution of the spectral method would be ~75 km). These sources are, by definition, wide and present long wavelengths in the magnetic signal. These long wavelengths are by well resolved with this line spacing configuration already mentioned above.

Additional changes

Since the initial submission, Rutishauser et al. 2017 (AGU abstract) has now been published as a journal paper, so we have added the full reference.

We have also added two extra references for: (i) context on GHF/basal water comparisons (Siegert and Dowdeswell 1996), (ii) Ground water (Siegert et al 2017).

We have changed the reference in the flow-routing methods section to Wang and Li 2006.

Manuscript prepared for The Cryosphere
with version 2015/04/24 7.83 Copernicus papers of the LaTeX class copernicus.cls.
Date: 22 June 2018

A constraint upon the basal water distribution and ~~basal~~ thermal state of the Greenland Ice Sheet from radar bed-echoes

Thomas M. Jordan[1,2], Christopher N. Williams[1,3], Dustin. M. Schroeder[2,4], Yasmina M. Martos[5,6], Michael A. Cooper[1], Martin. J. Siegert[7], John D. Paden[8], Philippe Huybrechts[9], and Jonathan L. Bamber[1]

[1]Bristol Glaciology Centre, School of Geographical Sciences, University of Bristol, Bristol, UK.
[2]Department of Geophysics, Stanford University, Stanford, CA, USA.
[3]Now at British Geological Survey, Nottingham, UK.
[4]Department of Electrical Engineering, Stanford University, Stanford, CA, USA.
[5]Department of Astronomy, University of Maryland, College Park, MD, USA.
[6]NASA Goddard Space Flight Center, Greenbelt, MD, USA.
[7]Grantham Institute and Department of Earth Science and Engineering, Imperial College, London, UK.
[8]Center for Remote Sensing of Ice Sheets, University of Kansas, Lawrence, USA.
[9]Earth System Science and Departement Geografie, Vrije Universiteit Brussel, Brussels, Belgium.

Abstract. There is widespread, but often indirect, evidence that a significant fraction of the bed beneath the Greenland Ice Sheet is thawed (at or above the pressure melting point for ice). This includes the beds of major outlet glaciers and their tributaries and a large area around the North-GRIP borehole in the ice-sheet interior. The ice-sheet scale distribution of basal water is, however, poorly constrained by existing observations. In principle, airborne radio-echo sounding (RES) enables the detection of basal water from bed-echo reflectivity, but unambiguous mapping is limited by uncertainty in signal attenuation within the ice. Here we introduce a new, RES diagnostic for basal water that is associated with wet-dry transitions in bed material: bed-echo reflectivity variability. This technique acts as a form of edge detector and is a sufficient, but not necessary, criteria for basal water. However, the technique has the advantage of being attenuation-insensitive and suited to data combination, enabling combined analysis of over a decade of Operation IceBridge survey data. ~~Importantly, this diagnostic is demonstrated to be attenuation-insensitive and suited to data combination, enabling combined analysis of over a decade of Operation IceBridge survey data.~~

The basal water predictions are compared with existing analyses of the basal thermal state (frozen and thawed beds) and geothermal heat flux. In addition to the outlet glaciers, we demonstrate widespread water storage in the northern and eastern interior. Notably, we observe a quasi-linear 'corridor' of basal water extending from NorthGRIP to Petermann glacier that ~~spatially~~ correlates spatially with elevated heat flux predicted by a recent magnetic model. Finally, with a general aim to stimulate regional- and process-specific investigations, the basal water predictions are compared

with bed topography, subglacial flow paths, and ice-sheet motion. The basal water distribution, and its relationship with the basal thermal state, provides a new constraint for numerical models.

1 Introduction

Basal water beneath the Greenland Ice Sheet (GrIS) influences, and is influenced by, the dynamics and thermodynamics of the overlying ice. A lubricated bed is a necessary condition for basal sliding, which can be responsible for up to about 90% of the ice surface velocity (van der Veen, 2013). Constraining the spatial distribution of basal water is important, therefore, for understanding the dynamic state of the overlying ice and its sensitivity to external forcing. A reliable estimate of the presence of basal water can also be used as a boundary condition/constraint in numerical modelling and to evaluate model performance and is, as a consequence, an attractive objective.

The spatial distribution of basal water beneath the GrIS is known to arise from an interplay of different physical processes including: surface melt (e.g. van de Wal et al. (2008)), basal melting due to geothermal heat (e.g. Dahl-Jensen et al. (2003); Rogozhina et al. (2016)), frictional and shear heating (e.g. van der Veen (2013)), and transport processes (surface, englacial and subglacial) which redistribute water (e.g. Rennermalm et al. (2013); Chu (2014)). There are, however, limited observational constraints on the ice-sheet scale distribution of basal water, and the relationship with other glacial and subglacial properties is therefore largely unexplored and/or speculative. The lack of unambiguous information about basal water arises primarily because there are only a few existing observations of subglacial lakes (Palmer et al., 2013; Howat et al., 2015; Willis et al., 2015; Palmer et al., 2015). By contrast, the Antarctic Ice Sheet currently has over 400 identified subglacial lakes (Siegert et al., 2016)) some of which have been found to be actively draining/recharging. Instead, there is evidence that basal water beneath the GrIS exists in smaller pools (Chu et al., 2016), as wet sediment (Christianson et al., 2014), and as part of channelised networks (Livingstone et al., 2017).

The basal temperature distribution of the GrIS determines where basal water can exist, and requires basal temperatures at or above the pressure melting point (PMP) for ice (from herein 'thawed'). Direct basal temperature measurements are, however, sparse. At the majority of the interior boreholes - Camp Century, Dye 3, GRIP, GISP2, and NEEM - basal temperatures indicate frozen beds (Weertman, 1968; Gundestrup and Hansen, 1984; Dahl-Jensen et al., 1998; Cuffey et al., 1995; MacGregor et al., 2016), with the thawed bed at NorthGRIP an exception (Andersen et al., 2004). Toward the ice-sheet margins boreholes generally indicate thawed beds (MacGregor et al., 2016). Indirect methodologies for discriminating frozen and thawed beds (ice-sheet model predictions, radiostratigraphy, and surface properties) were recently combined by MacGregor et al. (2016), to produce a frozen-thawed likelihood map for beds beneath the GrIS. Key predictions were that the central ice divides and west facing slopes generally have frozen beds, the southern and western outlet glaciers have a thawed bed, and that basal thaw extends east from NorthGRIP over a large fraction of the northeastern ice sheet.

Spatially variable geothermal heat flux (GHF) influence the basal temperature distribution (Dahl-Jensen et al., 2003; Greve, 2005; Rogozhina et al., 2016), hydrology (Rogozhina et al., 2016), and flow features (Fahnestock et al., 2001) in the interior of the GrIS. Notably, the onset of the North East

Greenland Ice Stream (NEGIS) is predicted to arise from basal melting that is attributed to locally elevated GHF (Fahnestock et al., 2001), which, in turn, has recently been attributed to the path of the Iceland hotspot track (Rogozhina et al., 2016; Martos et al., In revision). As with basal temperature, the sparsity of borehole measurements limits direct inference of GHF (which is related to the vertical gradient of basal temperature). Instead, a range of geophysical techniques including: tectonic (Pollack et al., 1993), seismic (Shapiro and Ritzwoller, 2004), and magnetic (Fox Maule et al., 2009; Martos et al., In revision) models have been used to map GHF beneath the ice sheet. These models, however, differ greatly in the predicted spatial distribution for GHF and also in the absolute values (Rogozhina et al., 2012). Due to the relationship between basal melt and GHF, basal water observations can be used to further refine and cross-validate GHF models (Siegert and Dowdeswell, 1996; Schroeder et al., 2014; Rogozhina et al., 2016).

In principle, airborne radio-echo sounding (RES) surveys provide the information and spatial coverage to infer the presence of basal water at the ice-sheet scale. Bed-echo reflectivity is the most commonly used diagnostic for this purpose (e.g. Peters et al. (2005); Jacobel et al. (2009); Oswald and Gogineni (2008)), and is based upon the prediction that, across a range of subglacial materials, wet glacier beds have a higher reflectivity than dry or frozen beds (Bogorodsky et al., 1983; Martinez et al., 2001; Peters et al., 2005). However, due to uncertainty and spatial variation in radar attenuation (an exponential function of temperature (Corr et al., 1993)) bed-echo reflectivity is subject to spatial bias and can be ambiguous when mapped over larger regions (Matsuoka, 2011; MacGregor et al., 2012; Jordan et al., 2016). In order to mitigate spatial bias from radar attenuation, bed-echo scattering properties - including the 'specularity' (a measure of the angular distribution of energy and, consequently, the smoothness of the bed at a radar-scale wavelength) (Schroeder et al., 2013; Young et al., 2016) and the bed-echo 'abruptness' (a waveform parameter) (Oswald and Gogineni, 2008, 2012) - have also been employed in basal water detection. Although attenuation-independent, use of some bed-echo scattering properties to discriminate basal water can be prone to ambiguity and can potentially lead to false-positive detection of smoother bedrock as water (Jordan et al., 2017).

In this study we introduce a RES diagnostic for basal water that is specifically tuned to be suitable for an ice-sheet scale assessment of basal thaw. The RES diagnostic, which we term 'bed-echo reflectivity variability', detects wet-dry transitions in bed material and acts as a form of edge detector. The technique is demonstrated to be insensitive to radar attenuation, thus reducing the likelihood of false-positive identification of basal water at the ice-sheet scale. Moreover, it also only requires local radiometric power calibration, and thus enables different Operation IceBridge RES campaigns, using different radar system settings (e.g. peak transmit power, antenna gain), to be combined and mapped. However, a limitation of the technique is that it provides a sufficient (not necessary) condition for basal water, and the detected subset of basal water corresponds to sharp transitions/horizontal gradients in the bed dielectric. ~~Whilst only encompassing a subset of basal water (specifically, finite water~~

~~bodies with sharp horizontal gradients in water content) the RES diagnostic enables a new ice-sheet scale constraint to be placed upon where the bed of the GrIS is thawed.~~ The primary geographical focus of the study is ~~therefore~~to compare the spatial relationship between predicted basal water and up-to-date analyses for the basal thermal state (MacGregor et al., 2016) and GHF (Shapiro and Ritzwoller, 2004; Fox Maule et al., 2009; Martos et al., In revision) beneath the GrIS. We observe new predictions for basal water predominantly in the northern and eastern ice sheet, which spatially correlate with elevated GHF recently inferred by Martos et al. (In revision). We then compare basal water and bed topography (Morlighem et al., 2017), which enables us to identify likely subglacial flow paths and storage locations beneath the contemporary ice sheet. Finally, with a view toward improving our understanding of the influence of basal water upon ice-sheet motion, we compare the relationship between basal water and ice surface speed (Joughin et al., 2010, 2016).

2 Methods

2.1 Radio-echo sounding data and bed-echo analysis

The airborne RES data used in this study were collected by the Center for Remote Sensing of Ice Sheets (CReSIS) over the time period from 2003-2014. The data were taken using a succession of radar instruments: Advanced Coherent Radar Depth Sounder (ACORDS), Multi-Channel Radar Depth Sounder (MCRDS), Multi-Channel Coherent Radar Depth Sounder (MCoRDS), Multi-Channel Coherent Radar Depth Sounder: Version 2 (MCoRDS v2), mounted on three airborne platforms: P-3B Orion (P3), DHC-6 Twin Otter (TO) DC8, Douglas DC-8 (DC8) (Paden, 2015). The flight-track coverage, subdivided by radar system, is shown in Fig. 1(a) with the season breakdown: ACORDS 2003 P3 and 2005 TO; MCRDS 2006 TO, 2007 P3, 2008 TO and 2009 TO; MCoRDs 2010 P3 and 2010 DC8; MCoRDs v2 2011 TO, 2011 P3, 2012 P3, 2013 P3, 2014 P3. More details on the track lengths and data segmentation can be found in MacGregor et al. (2015a). The vast majority of the data were collected in the months March-May.

The various radar system details and signal processing steps are described in detail in previous works (Rodriguez-Morales et al., 2014; Gogineni et al., 2014; Paden, 2015). The centre-frequency of the radar systems is either 150 MHz (ACORDS and MCRDS) or 195 MHz (MCoRDs and MCoRDS v2), and, after accounting for pulse-shaping and windowing, the depth-range (vertical) resolution can vary from $\sim$ 4.3-20 m in ice. The along-track (horizontal) resolution also varies between field seasons, and is typically $\sim$ 30 or 60 m. The radar-echo strength profiles (CSARP, Level 1B data) employ fixed fast-time gain where the receiver gain is constant for each recorded pulse which enables consistent interpretation of bed-echo power on a season-by-season basis. Whilst transmitted power can differ between seasons, since we consider local variability, offsets between seasons do not matter which enables straightforward inter-season data combination. Pre-2003 CReSIS data uses manual gain control and hence these seasons are not included.

The procedure to extract bed-echo power is similar to Oswald and Gogineni (2008); Jordan et al. (2016, 2017) and aggregates power over bed-echo fading (i.e. performs a depth-range integral). Briefly, the procedure consists of the following steps. Firstly, CReSIS ice thickness (Level 2) picks were used as initial estimate for the depth-range bin of the peak bed-echo power. Secondly, a local re-tracker wqas used to locate the true depth-range bin for peak bed-echo power. Thirdly, the power was aggregated by a discrete summation over the bed-echo envelope (both before and after the peak). The summations were truncated when the power was 10 dB or less than the peak, thus to ensure that the integral consists of a dominant peak associated with a dominant reflecting facet. The chosen SNR threshold of 10 dB in this study is less strict than the $\sim$ 17 dB threshold used in Jordan et al. (2016, 2017), and was required to extend the effective coverage to some interior regions in southern Greenland. Additionally, in this study we did not apply along-track averaging of L1B data as was done previously. Finally, again, to ensure a suitable signal-to-noise ratio, a 'quality control' measure is imposed such that bed-echo peak power must be 10 dB above the noise floor. This results in the effective coverage shown in Fig. 1(b). Regions with 'poor' quality bed-echoes include a spatially coherent coverage gap in the southern interior, high altitude data, and some marginal regions.

The rationale for use of aggregated bed-echo power (over peak power) is that it serves to reduce bed-echo power variability due to roughness, and thus better enables comparison with the specular bed-echo reflectivity values that are used to infer bulk material properties (Oswald and Gogineni, 2008). Additionally, since roughness scattering loss is frequency-dependent (MacGregor et al., 2013), aggregated power serves as a pragmatic way to best combine bed-echo power measurements from the 195 MHz and 150 MHz radar systems. This is supported by the observed $\sim$ 1 dB greater scattering loss (estimated here by the dB difference between peak and aggregated power) for the 195 MHz systems at cross-over points.

Key landmarks of the GrIS that are used in the data description - temperature boreholes, drainage basin boundaries, and major fast flow regions - are shown in Fig. 1(c).

2.2 Bed-echo power, attenuation correction and bed-echo reflectivity

The bulk material properties of glacier beds, including the presence of basal water, can, in principle, be inferred from the reflectivity of the bed-echo (Bogorodsky et al., 1983; Peters et al., 2005). The reflectivity, $[R]$, is obtained from solving the decibel form of the bed-echo power equation

$$[P] = [S] - [G] + [R] - [L] - [B], \tag{1}$$

where $[P]$ is the bed-echo power (in this case the aggregated bed-echo power, which mitigates for scattering losses from the ice-bed interface), $[S]$ is the system performance, $[G]$ is the geometric correction, $[L]$ is the attenuation loss in ice, and $[B]$ is the loss due to birefringence (ice fabric anisotropy), and the notation $[X] = 10\log_{10} X$ is assumed (Matsuoka et al., 2010). Rough surface losses from transmission through the air-ice interface (e.g. Grima et al. (2014); Schroeder et al.

(2016a)) also influence the radar power budget, and are discussed in more detail in Sect. 4.6. The geometric correction for a specular reflector can be defined by

$$[G] = 2[2(s + h/\sqrt{\epsilon_{ice}})], \tag{2}$$

where s is the aircraft height and h is the ice thickness and $\epsilon_{ice} = 3.15$ is the relative dielectric permittivity of ice to give the geometrically-corrected bed-echo power

$$[P_g] = [P] + [G]. \tag{3}$$

(e.g. Schroeder et al. (2016a)). For the majority of the CReSIS data used (2006 TO onward) s and h are known and eq. (2) can be applied exactly. For the 2003 P3 and 2005 TO seasons only h is known and s = 500 m is assumed (approximately the mean aircraft height). This approach is justifiable since in this study we are interested in local (length scale $\sim$ 5 km) power variation, where s varies slowly. It is assumed that variation in $[S]$ and $[B]$ is also negligible (again, approximations that are strengthened by consideration of local power variation) then eq. (1) reduces to

$$[P_g] = [R] - [L], \tag{4}$$

where $[P_g] = [P] + [G]$ is geometrically-corrected bed-echo power. Finally, setting $[L] = 2 < N > h$ gives

$$[P_g] = [R] - 2 < N > h, \tag{5}$$

where $< N >$ (dB km^{-1}) is the (one-way) depth-averaged attenuation rate (Matsuoka et al., 2010).

A fundamental ambiguity in bed-echo reflectivity analysis is that there are two unknowns in eq. (5): $< N >$ and $[R]$. Two approaches are typically used to determine $< N >$: (i) 'forward modelling' using estimates of attenuation as a function of englacial temperature (e.g. MacGregor et al. (2007); Matsuoka et al. (2012b); Chu et al. (2016)), (ii) 'empirical-determination' using the linear regression of bed-echo power and ice thickness (e.g. Jacobel et al. (2009); Schroeder et al. (2016b)). Attenuation follows an Arrhenius (exponential) relationship with temperature and a linear dependence upon the concentration of ionic impurities: primarily hydrogen (H^+), but also chlorine (Cl^-), and ammonium (NH_4^+) (Corr et al., 1993; Wolff et al., 1997; MacGregor et al., 2007, 2015b). On an ice-sheet scale, the uncertainty when 'forward' modelling $< N >$ is so high that it can be prohibitively challenging to accurately calibrate $[R]$ (Matsuoka et al., 2012a; MacGregor et al., 2015b; Jordan et al., 2016). This is due to both uncertainty in ice-sheet model temperature fields, the ionic concentrations, and the tuning of the parameters in the Arrhenius equation (MacGregor et al., 2007, 2015b). Empirical determination of $< N >$ using bed-echo power is also subject to sources of potential bias. In particular, the regression methods can be ill-posed when there is rapid spatial variation in attenuation (Matsuoka et al., 2012a), or when there is a thickness-correlated distribution in bed-echo reflectivity (Jordan et al., 2016).

We will later demonstrate that, unlike absolute values of $[R]$, local variability in bed-echo reflectivity is highly insensitive to modelled values of $< N >$ (Sect. 2.6). However, despite acting as a very weak constraint, an initial estimate for ice-sheet scale variation in $< N >$ is still necessary to calculate reflectivity variability. The estimate for $< N >$ relies on previous work by Jordan et al. (2016) and uses the 'M07' Arrhenius equation MacGregor et al. (2007), the Greenland Ice Sheet Model (GISM) temperature field from Huybrechts (1996) as updated in Goelzer et al. (2013), depth-averaged ionic concentrations from the GRIP ice core (MacGregor et al., 2015b), and the Greenland ice thickness data set in Bamber et al. (2013a). The temperature field derives from a full 3D thermomechanical simulation over several glacial-interglacial cycles and is subsequently rescaled to a 1 km representation of the Bamber et al. (2013a) ice thickness. The geothermal heat flux in GISM was initially taken from Shapiro and Ritzwoller (2004) but further adjusted with Gaussian functions around the deep ice core sites to match observed basal temperatures. Vertical temperature profiles are within 1-2°C when compared to available in-situ measurements. GISM resolves the flow on a model resolution of 5 km, which causes some smoothing of the temperature field in narrow outlet glaciers near to the coast.

Using this model framework, it is that predicted that $< N >$ varies by a factor ~ 5 over the GrIS, ranging from ~ 6 dB km^{-1} in the colder northern interior to ~ 30 dB km^{-1} toward the warmer southwestern margins (refer to Fig. 5(a) in Jordan et al. (2016) for a spatial plot).

2.3 Calculating bed-echo power and reflectivity variability

We have now substantially revised this section in response to the second reviewer's comments. Key changes include: (i) a revised intro to the section being more up-front about the purpose/rationale for the approach, (ii) a motivation of statistics in dB space ,(iii) A comparison with previous literature that considered along-track variability in peak power.

In this study we use simple standard deviation measures to quantify the variability of bed-echo power and reflectivity along the flight-tracks, notated by: $\sigma_{[P_g]}$ and $\sigma_{[R]}$. The numerical calculation is analogous to how topographic roughness (the rms height) is calculated from bed elevation profiles (Shepard et al., 2001), and assumes an along-track 'window' of length 5 km evaluated at 1 km intervals (taking the standard deviation of all the points within the the window). The choice of horizontal length scale was chosen for consistency with the basal thermal state mask by MacGregor et al. (2016), which was deemed an appropriate scale for integration of radar data with thermomechanical models at the ice-sheet scale. At this 5 km length scale, high values of reflectivity variability - a diagnostic for dielectric/wet-dry transitions (also,see Sect. 2.5) - act as a form of edge detector. The rationale for using this approach (rather than a conventional edge detector) is that it does not impose that a single along-track transition is present, which is desirable when aiming to also detect mutliple smaller water bodies relative to the window size.

Since this application of along-track variability is a non-standard approach to bed-echo data analysis, we now take a closer look at the statistical properties. The formula for $\sigma_{[P_g]}$ follows from the variance of eq. (4) and is given by

$$\sigma_{[P_g]} = \sqrt{\sigma^2_{[R]} + \sigma^2_{[L]} - 2\sigma_{[R],[L]}}, \tag{6}$$

where $\sigma_{[L]}$ is the standard deviation in attenuation loss, and $\sigma_{[R],[L]}$ is the covariance of bed-echo reflectivity and attenuation loss. Using $[L] = 2 < N > h$ and assuming $< N >$ can be approximated as constant (justifiable at the 5 km length scale that is ~~later~~ considered) then eq. (6) becomes

$$\sigma_{[P_g]} = \sqrt{\sigma^2_{[R]} + 4 < N >^2 \sigma^2_h - 4 < N > \sigma_{[R],h}}, \tag{7}$$

where σ_h is the standard deviation of ice thickness and $\sigma_{[R],h}$ is the covariance of bed-echo reflectivity and ice thickness. Equations (6) and (7) consider the variability of log-transformed variables (i.e. the dB/additive form of the radar power equation). This differs from the variability of the linear variables (i.e. the multiplicative form of the radar power equation) expressed in log space. The first advantage to our use of log-transformed variables is that we can better separate the variability contributions into separate components. The second advantage is that we can make a clearer connection to the dB reflection amplitudes that are typically used in radioglaciology (Bogorodsky et al., 1983; Peters et al., 2005). This includes prior applications that have considered the distribution and standard deviation of dB reflection amplitudes in the context of water detection (Wolovick et al., 2013; MacGregor et al., 2013).

In regions where $\sigma_{[R],[L]} \approx 0$, (bed-echo reflectivity has negligible covariance with attenuation loss), eq. (6) and eq. (7) are approximated by

$$\sigma_{[P_g]} \approx \sqrt{\sigma^2_{[R]} + \sigma^2_{[L]}}, \tag{8}$$

$$\approx \sqrt{\sigma^2_{[R]} + 4 < N >^2 \sigma^2_h}, \tag{9}$$

and the loss component of $\sigma_{[P_g]}$ is solely modulated by $\sigma_{[L]}$ which is proportional to the product $< N > \sigma_h$. Whilst an approximation (in certain circumstances the second and third terms on the right hand side of eq. (6) and eq. (7) can be of comparable magnitude) this scenario provides an intuitive way to understand the interrelationship between $\sigma_{[P_g]}$, $\sigma_{[R]}$ and $\sigma_{[L]}$.

Two example profiles for $[P_g]$, $\sigma_{[P_g]}$, $[R]$, $\sigma_{[R]}$, $[L]$, $\sigma_{[L]}$ and h are shown in Fig. 2. Fig. 2(a) is a representative example from the interior of the ice sheet where $\sigma_{[L]}$ is relatively low and h is thick ($\sim$ 2.8 km). Subsequently the profiles for $\sigma_{[P_g]}$ and $\sigma_{[R]}$ are very similar in appearance, with the most notable difference at distance $\sim$ 360 km where there is higher $\sigma_{[P_g]}$ due to the subglacial trough. The peaks in $\sigma_{[R]}$ are later related to wet dry bed material transitions in Sect. 2.5. It is also important to note that $\sigma_{[R]}$ can be greater than $\sigma_{[P_g]}$ (e.g. at distance $\sim$ 342 km), which is an effect that can be explained by the covariance between attenuation loss/ice thickness and bed-echo reflectivity in eq. (6) and eq. (7)). Fig. 2(b) is a representative example from toward the ice-sheet margins

where $\sigma_{[L]}$ is higher due to more rapid variation in h (more complex bed topography) and higher values of $< N >$ (warmer ice). In this case, $\sigma_{[P_g]}$ is noticeably greater than $\sigma_{[R]}$, with the differences largely attributable to higher $\sigma_{[L]}$ as anticipated by eq. (8). The examples in Fig. 2 highlight that, at this length scale, higher values of $\sigma_{[R]}$ ~~can~~ arise primarily due to a large single transition in $[R]$. However, there are also instances where multiple transitions result in local variability peaks (e.g. at distance $\sim$ 380-385 km along 2(a)). ~~due to either a large single transition in $[R]$, multiple smaller transitions/fluctuations, or a combination of both signal components. The physical consequences and interpretation of the 5 km length scale in the context of water detection is discussed in Sect. 2.5.~~

When calculating $\sigma_{[P_g]}$, $\sigma_{[R]}$ and $\sigma_{[L]}$, bed-echo coverage gaps within a 5 km bin (see Fig. 1(b)) were accounted for by neglecting bins where less than half the data corresponded to 'good' bed-echoes. The effects of this filtering step are demonstrated in Fig. 2(b) where, aligned with the deep subglacial trough at distance $\sim$ 1324 km, there are along-track gaps in $\sigma_{[P_g]}$, $\sigma_{[R]}$ and $\sigma_{[L]}$.

It is important to clarify the difference between the use of bed-echo power/reflectvity variability in this study from previous radioglaciology studies (Neal, 1982; Peters et al., 2005; Carter et al., 2007; Grima et al., 2014). These studies focused upon the variability/statistics of the peak echo power as a result of phase modulation by interfacial roughness. By contrast, in this study we suppress roughness effects by integrating power in fast time over the echo envelope (Sect. 2.1). We are therefore able to focus upon power variability that is a result of along-track changes in the bed dielectric.

2.4 Distributions for bed-echo power and reflectivity variability

Spatial distributions for the variability measures: $\sigma_{[P_g]}$, $\sigma_{[L]}$, $\sigma_{[R]}$ are shown in Fig. 3(a,b,c). To aid the interpretation ice thickness (Morlighem et al., 2017) is shown in Fig. 3(d). In general, $\sigma_{[P_g]}$ has a strong ice thickness dependence, and increases toward the margins where ice is thinner. The attenuation correction, which primarily acts to reduce the component of $\sigma_{[P_g]}$ that is attributable to $\sigma_{[L]}$, results in a more uniform ice-sheet scale distribution of $\sigma_{[R]}$ than $\sigma_{[P_g]}$. Notably, there are localised patches of higher $\sigma_{[R]}$ present in both marginal and interior regions (which are later attributed to the presence of basal water). The ice-sheet scale trends in $\sigma_{[P_g]}$ and $\sigma_{[L]} = 2 < N > \sigma_h$ can be related to spatial variation in $< N >$ (MacGregor et al., 2015b; Jordan et al., 2016) and bed roughness (Rippin, 2013; Jordan et al., 2017) (which correlates with σ_h) .

The two zoom regions in Fig. 3 include the flight-track profiles in Fig. 2. (north-central ice sheet, pink bounding box; northwestern margins, black bounding box). These examples serve to further illustrate the spatial interrelationship between $\sigma_{[P_g]}$, $\sigma_{[R]}$ and $\sigma_{[L]}$ in a typical interior region with lower $\sigma_{[L]}$ and a typical marginal region with higher $\sigma_{[L]}$. Its is clear that the interior example has very similar spatial distributions for $\sigma_{[P_g]}$ and $\sigma_{[R]}$, whereas the marginal example has higher $\sigma_{[P_g]}$ associated with the higher $\sigma_{[L]}$ that occurs in the subglacial troughs and more complex topography toward the edge of the ice sheet. The marginal example also demonstrates that the power variability associated with the subglacial troughs is largely removed for $\sigma_{[R]}$.

The corresponding frequency distributions for $\sigma_{[P_g]}$ and $\sigma_{[R]}$ are shown in Fig. 4. Both demonstrate a strong positive-skew, with a long-tail extending to higher values. The mean and standard deviation for $\sigma_{[P_g]}$ is greater than $\sigma_{[R]}$. This is consistent with the commonly observed result that making an attenuation correction to $[P_g]$ acts to reduce the overall decibel range for $[R]$, (e.g. Oswald and Gogineni (2008); Schroeder et al. (2016b)), hence more closely resembling the predicted dB range for bed materials (Peters et al., 2005).

A quantification and discussion of cross-over statistics for $\sigma_{[R]}$ is given in Appendix A.

2.5 Interpretation of reflectivity variability as a ~~diagnostic~~ sufficient diagnostic for basal water

Radar bed-echo reflectivity depends upon the dielectric contrast between glacier ice and bed material. For a specular, nadir reflection the Fresnel power reflection coefficient is given by

$$[R] = 10\log_{10}\left|\frac{\sqrt{\tilde{\epsilon_{bed}}}-\sqrt{\tilde{\epsilon_{ice}}}}{\sqrt{\tilde{\epsilon_{bed}}}+\sqrt{\tilde{\epsilon_{ice}}}}\right|^2, \tag{10}$$

where $\tilde{\epsilon_{ice}}$ and $\tilde{\epsilon_{bed}}$ are the complex dielectric permittivity of the glacier ice and bed material respectively. The relative (real) part of the permittivity, ϵ_{bed}, is the primary control upon $[R]$. A summary of dielectric and reflective properties of glacier bed materials at typical ice-penetrating radar frequencies is given in Table 1 and is collated from Bogorodsky et al. (1983); Martinez et al. (2001); Peters et al. (2005). The permittivity and reflectivity range for each material arises due to sub-wavelength dielectric mixing between either ice or water and the bed material, and takes into account typical saturation and porosity values (Martinez et al., 2001; Peters et al., 2005). In general, lower values of ϵ_{bed} and $[R]$ occur for dry or frozen bed materials (approximately $\epsilon_{bed} < 7$ and $[R] <$ -14 dB), whilst higher values occur for wet bed materials (approximately $\epsilon_{bed} > 7$ and $[R] >$ -14 dB). Dielectric mixing between bed materials can also occur at the length scale of the Fresnel zone ($\sim$ 100 m), which results in a further averaging of the observed reflectivity (Berry, 1975; Peters et al., 2005).

Due to the range of possible bed materials at the ice-sheet scale it is not possible to formulate a unique dielectric model for diagnosing water from $\sigma_{[R]}$. A simple 'two-state' dielectric model, does, however, enable us to physically motivate the water diagnostic in terms of dielectric properties (Fig. 5). The model assumes that the along-track sample window is comprised of two different bed materials: the dry 'background' bed material with permittivity ϵ_{dry} and reflectivity $[R_{dry}]$, and the wet material with permittivity ϵ_{wet} and reflectivity $[R_{wet}]$. For simplicity, it is assumed that each along-track measurement is in one of the wet or dry states, with the wet-dry mixing ratio parameterised by f. In this formulation, a single body of wet material or multiple smaller bodies of wet material, have the same formula for the reflectivity variability given by

$$\sigma_{[R]} = \Delta[R]\sqrt{f^2(1-f)+(1-f)^2 f}, \tag{11}$$

where $\Delta[R] = [R_{wet}] - [R_{dry}]$ is the reflectivity difference between wet and dry beds. Eq. (11) is derived by considering the weighted variance for two discrete random variables and does not account for non-linear variations due to variable scattering coherence. A phase-space plot for $\sigma_{[R]}(f, \Delta[R])$ is shown in Fig. 5(c), and shows that for fixed $\Delta[R]$, $\sigma_{[R]}$ is maximised when f = 0.5 (i.e. an even mixing of wet and dry materials).

Past diagnosis of basal water typically associates the upper tail of the reflectivity distribution with water, prescribing a threshold above which the bed is interpreted as wet (e.g. Jacobel et al. (2009); Chu et al. (2016)). In this study, a similar thresholding approach is applied to the distribution of $\sigma_{[R]}$ (Fig. 4(b)). The threshold choice for basal water ($\sigma_{[R]}$ > 6 dB) corresponds to the region greater than the $\sigma_{[R]}$ = 6 dB contour in Fig. 5(c) and requires a minimum wet-dry reflectivity difference of $\Delta[R]$ > 12 dB. In general, $\Delta[R]$ > 12 dB is only possible for a mixture of wet and dry (or frozen) bed materials (Table 1). For example, an even mixing of ground water and dry granite (f = 0.5, $\Delta[R]$ = 17 dB) has $\sigma_{[R]}$ = 8.5 dB. The contours in Fig. 5(c) demonstrate that small perturbations to even mixing (f $\neq$ 0.5) produce similar $\sigma_{[R]}$, and hence that water detection is insensitive to the discretisation of the along-track sample window (Sect. 2.3). Overall, the threshold choice ($\sigma_{[R]}$ > 6 dB) is fairly conservative and is deliberately intended to reduce false-positive detection of basal water (at the expense of reduced overall detection). Finally, as discussed in Sect. 2.3, the 6 dB variability threshold applies to the distribution of log-transformed reflectivity.

The bed-echo power aggregation in Sect. 2.1 partially mitigates for roughness-induced scattering loss and the along-track power variability associated with this. Supporting evidence is that the cross-over analysis for $\sigma_{[R]}$ (see Appendix A) demonstrates there to be no significant bias for the 150 MHz radar systems (ACORDS and MCRDS) versus MCORDS v2 (the 195 MHz radar system used as a benchmark). ~~Additionally, we later demonstrate that the water detection method/semi-empirical threshold is well tuned to...~~. Additionally, whilst small-scale roughness transitions (transitions from specular to diffuse scattering) will often correlate with wet-dry transitions, this scenario will act to amplify the useful signal component with the $\sigma_{[R]}$ value increasing.

Finally, Table 1 also indicates that, in exceptional circumstances, $\Delta[R]$ > 12 dB could be generated in frozen/dry regions that partially contain sandstone or till that is close to matching the permittivity of ice. However, if present, these regions are likely to have indistinct bed-echoes and will not be included in the effective coverage in Fig. 1(b).

2.6 Basal water distribution and robustness to attenuation model bias

The initial basal water predictions ($\sigma_{[R]}$ > 6 dB) are shown in Fig. 6 (red, blue and green data), and correspond to $\sim$ 3.5 % of bins containing predominantly 'good' quality bed-echoes (Fig. 1(b)). A full geographic analysis of the spatial distribution is performed in Sect. 3. To demonstrate the robustness of the predictions, we performed a sensitivity analysis with respect to the modelled attenuation correction $< N >$ (Sect. 2.2) The analysis considered a series of increasingly large (uniform,

multiplicative) perturbations to $< N >$ and then tested if $\sigma_{[R]}$ > 6 dB also held for the perturbed model. Examples of 'persistent' water predictions for $\pm$ 20 $\%$ (red and green data) and $\pm$ 50 $\%$ (red data) perturbations to $< N >$ are indicated. As the perturbation size increases this results in a slight decrease in the overall percentage of water predictions (corresponding to $\sim$ 2.6 $\%$ and 2.1 $\%$ of the along-track bins for $\pm$ 20 $\%$ and $\pm$ 50 $\%$ respectively).

The sensitivity analysis tests the robustness of the water predictions to a number of different physical scenarios. Firstly, inherent bias in the Arrhenius equation parameters. For example, an empirical correction similar to the uniform perturbation considered in Fig. 6 was proposed by MacGregor et al. (2015b) to model unaccounted frequency-dependence in the electrical conductivity. Secondly, bias in the model temperature field ($< N >$ is approximately equivalent to depth-averaged temperature). Thirdly, bias due to assumed ionic concentration values. It is hard to formally quantify the possible range of these uncertainties but, based upon solution variability for $< N >$ using ice-sheet model temperature fields (Jordan et al., 2016), $\pm$ 20 $\%$ is a reasonable estimate for temperature related uncertainty. Subsequently, in the comparison with other data sets in Sect. 3 the subset of red and green points in Fig. 6 is used. Inherent bias in the Arrhenius equation parameters could be significantly higher than temperature uncertainty (MacGregor et al., 2015b). However, since the spatial structure for the basal water distribution under the $\pm$ 50 $\%$ perturbation is largely preserved, this is unlikely to significantly alter the conclusions that are drawn.

It is important to emphasise the robustness of $\sigma_{[R]}$ with respect to uncertainty/model bias in $< N >$ (particularly compared with bed-echo reflectivity, $[R]$). An analogous sensitivity analysis by Jordan et al. (2016) demonstrated that systematic over and underestimates in $< N >$ lead to pronounced ice thickness-correlated biases in the distribution for $[R]$ in northern Greenland (Fig. B1 in the original paper).

3 Results

The basal water distribution is now compared with existing analyses for the basal thermal state (MacGregor et al., 2016) (Sect. 3.1), geothermal heat flux (GHF) (Shapiro and Ritzwoller, 2004; Fox Maule et al., 2009; Martos et al., In revision) (Sect. 3.2), bed topography and subglacial flow paths (Morlighem et al., 2017) (Sect. 3.3), and ice surface speed (Joughin et al., 2010, 2016) (Sect. 3.4). The basal water predictions are always indicated by red circles. In regional zoom plots the circles are fixed to be 5 km in diameter (a true representation of the along-track window size and the effective resolution of the radar method). In ice-sheet scale plots the buffer size of the water predictions are increased for visualisation purposes. The radar flight-tracks represent where there are 'good' bed-echoes (Fig. 1(b)), and hence indicate the effective coverage.

In interpreting the maps it is important to emphasise that the basal water predictions in this study correspond to a subset of flight-track data where basal water is present. Specifically, they correspond

to where there are rapid spatial transitions/gradients in the bed dielectric (i.e. small, finite, water bodies or the boundaries of larger water bodies). The predictions therefore act as a sufficient constraint upon the distribution of basal water rather than being a fully comprehensive flight-track map for water extent. Additionally, since the vast majority of the radar measurements were collected before the onset of summer surface melt, to a first approximation, the basal water predictions correspond to the winter storage configuration.

3.1 Comparison between basal water distribution and basal thermal state synthesis

In Fig. 7(a) the basal water predictions are underlain by the basal thermal state synthesis (frozen/thawed likelihood) map by MacGregor et al. (2016). The synthesis employed four independent methods: (i) assessment of thermomechanical model temperature fields, (ii) basal melting inferred from radiostratigraphy, (iii) basal motion inferred from surface velocity, (iv) basal motion inferred from surface texture. The four methods were then equally weighted, leading to a likelihood map for frozen beds, thawed beds, and uncertain regions. Importantly, the prediction did not utilise radar bed-echo data and is therefore independent of our basal water predictions.

The reflectivity variability water diagnostic enables a positive discrimination of basal thaw, since $\sigma_{[R]} > 6$ dB is deemed as a sufficient (but not necessary) criteria for basal water. Positive discrimination of frozen regions is not, however, possible. This is because low reflectivity variability ($\sigma_{[R]} <$ 6 dB) could correspond to many different scenarios: a frozen region, a drier region at or above the PMP, or a wet region that is smoothly varying in bed-echo reflectivity. Since basal water enables a positive discrimination of thaw, red circles in likely thawed (pink) regions indicate agreement and red circles in likely frozen (blue) regions indicate disagreement with the basal thermal state synthesis. Absence of basal water in likely frozen regions is an indicator of general consistency between the two methods.

There is general agreement (water in predicted thawed regions) for the beds of major outlet glaciers and their upstream regions. This includes Helheim, Kangerlussuaq, Jakobshavn, and the other fast flowing regions identified in Fig. 1(c). There is also general agreement between basal water and the extent of predicted thaw in the NEGIS drainage basin. Major regions of disagreement (water in predicted frozen regions) are highlighted in the zoom plots, Fig. 7(b)-(f). The most obvious disagreement is the quasi-linear 'corridor' of basal water in the north-central ice sheet (Fig. 7(d)). This feature tracks close to the central ice divides and extends from the NorthGRIP region in the south toward Petermann glacier in the north. There are also noticeable areas of disagreement to the north and east of the Camp Century borehole (Fig. 7(b)), in the far north (Fig. 7(c)), to the east of GRIP (Fig. 7(e)), and around Kangerlussuaq (Fig. 7(f)). There is also an absence of water in many predicted frozen regions indicating consistency. This includes parts of the southern interior, north of the NEGIS drainage basin, and the majority of the interior region between the Camp Century and NEEM boreholes.

3.2 Comparison between basal water distribution and geothermal heat flux models

The basal temperature of glacier ice is governed by surface temperature, GHF, strain heating from internal deformation, frictional heating, and diffusive and advective heat transport (e.g. van der Veen (2013)). In the interior of the ice sheet, close to the ice divides, GHF, vertical advection, and diffusion are the dominant processes which influence basal temperature. In this scenario, the thermodynamic (temperature) equation can be approximated by the classical Robin model which predicts that basal melting occurs when GHF is above a certain threshold. ~~However, more comprehensively determining the minimum GHF forcing required to produce basal melt requires coupling to ice-sheet flow models, and is anticipated to be~~. For typical values of interior ice thickness and surface accumulation rate, which controls the rate of vertical heat advection, the minumum GHF forcing for melt is anticipated to be $\sim$ 55-70 mW m^{-2} in the interior of the ice sheet (Dahl-Jensen et al., 2003; Greve, 2005; Buchardt and Dahl-Jensen, 2007). In the water-GHF comparison we therefore define 'elevated' GHF (i.e. likely to produce basal melt) as > 60 mW m $^{-2}$. This definition is also informed by the lower range of values, (37-50 mW m^{-2}) that are typically associated with non-altered ancient continental crust (Artemieva, 2006; Rogozhina et al., 2016).

In Fig. 8 the basal water predictions are underlain by three different GHF models: the seismic model by Shapiro and Ritzwoller (2004), and two models derived from magnetic anomalies by Fox Maule et al. (2009) and Martos et al. (In revision). The GHF model by Shapiro and Ritzwoller (2004) is based upon the correlation between a 3D tomographic model of the crust and mantle temperature. The GHF models by Fox Maule et al. (2009) and Martos et al. (In revision) are based on a thermal model of the lithosphere with the lower boundary defined by the Curie depth which is determined from magnetic anomalies. Martos et al. (2017) further describes this approach and the additional spectral processing method used to produce Fig. 8(c). An older tectonic GHF model by (Pollack et al., 1993) is not considered and a spatial plot for the GrIS can be found in Rogozhina et al. (2012) along with a discussion of the caveats of the different types of model. A summary of local GHF estimates using borehole temperature profiles and thermomechanical model inversions

In interpreting Fig. 8, we limit the comparison to the ice sheet interior where the spatial correlation between GHF and basal water should be strongest. The model by Shapiro and Ritzwoller (2004), Fig. 8(a), predicts low GHF (< 60 mW m $^{-2}$) over the vast majority of the central and northern interior. There is therefore no correlation between elevated GHF and basal water. The model by Fox Maule et al. (2009), Fig. 8(b), predicts elevated GHF around GRIP and the southern and eastern boundaries of the NEGIS basin and basal water is also present in this region. There is, however, no correlation between elevated GHF and basal water along the ice divides north of NorthGRIP. The model by Martos et al. (In revision), Fig. 8(c), exhibits strong overall spatial correlation between basal water and elevated GHF in the interior of the northern ice sheet. Notably, there is a striking correlation between elevated GHF and the quasi-linear 'corridor' of basal water that extends from NorthGRIP

toward Petermann glacier. All three models predict regions of elevated GHF in the southern interior including the Dye 3 region. However, there is only isolated radar evidence for basal water.

In the comparison between the flight-track water predictions and GHF distributions in Fig. 8 it is important to bear in mind that the GHF distributions are evaluated at a lower spatial resolution. For example, the resolution of the GHF distribution by Martos et al. (In revision) is a consequence of the spectral method (window size and overlap) which has an effective resolution of $\sim$ 75 km.

3.3 Comparison between basal water distribution, bed topography and subglacial flow paths

In Fig. 9 the basal water predictions are underlain by the most recent Greenland bed topography digital elevation model (DEM) (Morlighem et al., 2017). To motivate further discussion about water storage locations and hydrological connectivity, a predicted subglacial flow path network is also included. The network structure is governed by gradients in the hydraulic pressure potential (Shreve, 1972) which was calculated using the bed elevation and ice thickness surfaces at a grid cell resolution of 600 m (derived from Morlighem et al. (2017)). The flow-routing algorithm was implemented in ArcGIS using the inbuilt flow accumulation tool on a hydraulic potential surface that had been processed for sink removal using the method of Wang and Li (2006). ~~and the hydrological sink filling procedure ..~~. Likely hydrological flow paths were identified by excluding flow paths where ~~fewer than 50~~50 or fewer neighbouring cells cumulatively contribute to a given location.

Fig. 9 demonstrates that the vast majority of the basal water predictions are well aligned with predicted subglacial flow paths. This alignment is most visually pronounced toward the margins and zoom plots are shown for the Petermann catchment in Fig. 9(b) and northwestern margins in Fig. 9(c). Fig. 9(b) also demonstrates that basal water is present along sections of the 'mega-canyon' feature identified by Bamber et al. (2013b) - for example, north west of the intersection (80°N, 50°W). In the interior of the ice sheet, where the horizontal gradients in ice thickness are small, local minima/sinks in the hydraulic potential surface should correlate with topographic depressions. The water storage locations in the interior generally conform to this behaviour (Fig. 9(d)).

3.4 Comparison between basal water distribution and ice surface speed

In Fig. 10 the basal water predictions are underlain by ice surface speed (Joughin et al., 2016) which is based upon a temporal average from 1st December 1995 to 31 October 2015. The ice surface speed is determined using interferometric synthetic aperture radar (InSAR) as described in Joughin et al. (2010). Whilst there is a complex overall relationship between basal water and ice velocity, there are some clear spatial patterns. Notably, in the topographically less constrained northern and western outlet glaciers, basal water is often concentrated in the fast-flow onset regions and tributaries whilst it is absent from the main trunks. This behaviour is particularly evident for the Petermann glacier catchment (Fig. 10(b)). In the topographically more constrained southeastern outlet glaciers, there is widespread evidence for basal water storage in both the f ast flowing glacial troughs and upstream

regions. This includes both the Kangerlussuaq catchment and the tight network of subglacial troughs to the south (Fig. 10(c)), and the Helheim catchment (Fig. 10(d)).

In the interior of the ice sheet basal water is predicted near to the head of the NEGIS ice stream. However, basal water is also predicted in some of the slowest flowing regions of the ice sheet interior. Notably, close to the central ice divides between NorthGRIP and Petermann and north east of GRIP.

4 Discussion

4.1 Basal water, basal thermal state and temperature

The basal water distribution in this study and the basal thermal state synthesis by MacGregor et al. (2016) represent two independent approaches to predict where the bed beneath the GrIS is thawed. There is greatest agreement (basal water in likely thawed regions identified by MacGregor et al. (2016)) toward the ice margins where ice surface speed is generally higher. The most noticeable regions of disagreement (basal water in likely frozen regions identified by MacGregor et al. (2016)) all occur where the ice surface speed is low. This includes the north-central ice-divide (Fig. 7(d)), the region east of GRIP (Fig. 7(e)), and the region west of Kangerlussuaq (Fig. 7(f)). The regions of agreement/disagreement are, perhaps, unsurprising, since three of the four methods employed by MacGregor et al. (2016) - ice-velocity, surface texture and radiostratigraphy - associate basal thaw with present (or past) ice sheet motion. In general, a thawed bed is a necessary (but not sufficient) condition for appreciable basal motion, and there is likely to be a subset of thawed regions where basal motion is negligible. This subset naturally incorporates water/thaw near the ice divides (since driving stress is low), and in the eastern ice sheet (since ice flow is topographically constrained).

Another key difference between the water predictions in this study and the thaw predictions by MacGregor et al. (2016) is that their study employed techniques better tuned to identify continuous regions of basal thaw, whereas the basal water predictions are localised. This provides another means to reconcile regions of disagreement, since in some instances the basal water predictions may correspond to localised patches above the PMP in an otherwise frozen region. A final explanation for discrepancies, is that the model temperature fields included in the basal thermal state synthesis were often tuned around knowledge of GHF at the time (i.e. Shapiro and Ritzwoller (2004); Fox Maule et al. (2009)).

There is no evidence for basal water at the location of the temperature boreholes, which, based upon the resolution of our method, corresponds to within 5 km. Since high reflectivity variability is not necessary for thaw this is consistent with both frozen and thawed borehole temperatures. Water is, however, observed fairly close to two frozen boreholes: $\sim$ 10 km south of GRIP and $\sim$ 7 km northeast of Camp Century (Fig. 7). At GRIP this is less surprising, since the basal temperature is 6 degrees below the PMP (Dahl-Jensen et al., 1998; MacGregor et al., 2016) and GHF is likely to be elevated in this region (Fig. 8). The basal water predictions near Camp Century are more

surprising, since in the late 1960s basal temperatures were measured to be 11.8 degrees below the PMP (Weertman, 1968; MacGregor et al., 2016). One possible explanation, which was recently invoked to explain the presence of a lake less than 10 km from South Pole (where the bed is frozen), is that the basal water is yet to reach thermal equilibrium (Beem et al., 2017). Another possible explanation is that the presence of hypersaline water could result in a depression of the PMP. This situation arises at Lake Vida in East Antarctica (where liquid water exists at -13 °C) (Murray et al., 2012) and at Devon Ice Cap in the Canadian Arctic (Rutishauser et al., 2018).

4.2 Basal water and geothermal heat flux

The comparison between basal water and the different GHF models in Fig. 8 (Shapiro and Ritzwoller, 2004; Fox Maule et al., 2009; Martos et al., In revision) demonstrates greatest consistency with the distribution by Martos et al. (In revision). Notably there is a pronounced spatial correlation between elevated GHF and the new predictions of basal thaw in the northern ice sheet. A recent machine learning derived map for GHF beneath Greenland by (Rezvanbehbahani et al., 2017) is also consistent with there being extensive basal thaw in this region. However, establishing definitive attribution of regions of the basal melt to GHF forcing (rather than frictional and strain heating, low advection from colder ice above, and/or surface melt water storage) will require integration with thermomechanical ice-sheet models. The basal water predictions could also be used as a constraint in a wide variety of other numerical modelling contexts. Experiments with 3D models to reconstruct the full ice temperature history over the last glacial cycle(s) can constrain the minimum GHF required to produce basal melting at the predicted basal water locations (Huybrechts, 1996). Other studies include investigating the sensitivity of ice-sheet dynamics to the thermal boundary condition (Seroussi et al., 2013) or basal lubrication (Shannon et al., 2013), and thermal models of the underlying lithosphere (Rogozhina et al., 2016).

Recent analyses imply that much of the spatial variation in GHF beneath the northern GrIS can be explained by Greenland's passage over the Iceland mantle plume between roughly 35 and 80 million years ago (Rogozhina et al., 2016; Martos et al., In revision). The magnetic GHF map in Fig. 8(c), alongside gravity data (Bouger anomalies), was recently used to by Martos et al. (In revision), to infer the most likely passage of the hotspot track. The most likely predicted path (corresponding to going forwards in geological time) follows the quasi-linear region of elevated GHF in Fig. 8(c) from Petermann glacier to NorthGRIP, and follows a path previously anticipated by Forsyth et al. (1986). The spatial correlation between elevated GHF and the quasi-linear basal water 'corridor' provides an additional source of evidence for the predicted path.

4.3 Basal water, bed topography and subglacial flow paths

There is growing evidence that much of the present day subglacial flow path network beneath the GrIS is paleofluvial in origin. This includes the dendritic flow path networks in the Jakobshavn

(Cooper et al., 2016) and Humboldt catchments (Livingstone et al., 2017), along with the prominent 'mega-canyon' feature which extends from the NorthGRIP region in the south to Petermann glacier in the north (Bamber et al., 2013b). The comparison between the predicted flow paths and basal water in Fig. 9 enables a revised assessment of the hydrological flow paths that are likely to be utilised in the contemporary ice sheet. For example~~, when the mega canyon was first identified by ...~~ the ~~accompanying~~ flow routing analysis demonstrates that basal water originating in the Petermann catchment is likely to route through sections of the canyon toward the ice-sheet margins. Fig. 9(b) supports this hypothesis, since the there is evidence for basal water along the majority of the canyon. However, it is important to stress that more rigorously assessing hydrological connectivity will require incorporation of DEM uncertainty when performing the flow routing (e.g. Schroeder et al. (2014)) and use of a coupled hydrological ice flow model (e.g. Le Brocq et al. (2009)).

4.4 Basal water and ice-sheet motion

Both observational (e.g. Moon et al. (2014); Tedstone et al. (2013)) and theoretical studies (e.g. Creyts and Schoof (2009); Schoof (2010)) point toward a complex spatio-temporal relationship between basal water and ice surface speed in fast flowing regions of the ice sheet. This ultimately depends upon the details of how the subglacial drainage system responds to surface melt water. In interpreting the relationship between basal water and ice surface speed in Fig. 10 it is therefore essential to re-emphasise that the basal water predictions correspond to the winter storage (pre surface melt) configuration. ~~Nevertheless, the apparent absence of water in the main trunks of the fast moving outlet glaciers....~~

In addition to basal water and temperature, spatial variation in the underlying geology and lithology of the GrIS (notably, presence or absence of deformable sediment) will also influence ice-sheet motion. It is widely anticipated that much of the interior of the ice sheet is underlain by hard pre-Cambrian rocks, with more limited sedimentary deposits toward the margins (Dawes, 2009; Henriksen, 2008), and in the NEGIS drainage basin (Christianson et al., 2014). It is therefore entirely plausible that much of the basal water predicted in the interior lies upon a hard undeformable bed (particularly in the context of the igneous rock that would be associated with the geological remnants of the Iceland hotspot track) and therefore experiences little motion due to bed deformation.

4.5 Comparison with past RES analyses of basal water and disrupted radiostratigraphy in Greenland

Despite acknowledged calibration issues, due to both variable radar system performance and spatial variation in attenuation, the bed-echo reflectivity analysis of 1990s PARCA RES data by Layberry and Bamber (2001) anticipated some of the water predictions in this study. This includes prior basal water predictions in the NEGIS onset region, and the upstream areas of Kangerlussuaq, Petermann and Humboldt glaciers.

There is a mixed agreement between the basal water predictions in this study and those from Oswald and Gogineni (2008, 2012) who performed joint bed-echo reflectivity/scattering analysis of the 1990s PARCA data. In general, better agreement with our results occurs in smoother topographic regions in the ice-sheet interior such as close to the NorthGRIP borehole. Since the effects of spatial bias due to attenuation uncertainty are lower in the interior of the ice sheet, this is where bed-echo reflectivity as a water diagnostic should be more robust. Additionally, the water detection method proposed by Oswald and Gogineni (2008, 2012) will generally not be able to discriminate water in many outlet glaciers and tributaries including Petermann and the northwestern margins (Jordan et al., 2017). This is because these regions tend to exhibit a diffuse scattering signature (associated with fine-scale roughness) whereas the method proposed by Oswald and Gogineni (2008, 2012) is specifically tuned to detect water bodies that exhibit a spatially continuous, (near-) specular scattering signature. By contrast, comparison between the water predictions in this study and the radar-derived bed roughness maps in Rippin (2013); Jordan et al. (2017) demonstrate a lack of modulation by bed roughness, with basal water present in rougher marginal regions and the generally smoother ice-sheet interior.

Basal units of disrupted radiostratigraphy are widely present in Greenland RES data sets (Bell et al., 2014; Wolovick et al., 2014; Bons et al., 2016; Dow et al., 2018). The features have been attributed to a supercooling 'freeze-on' process (Bell et al., 2014), 'stick-slip' mechanisms, (Wolovick et al., 2014) and the rheological anisotropy of ice (Bons et al., 2016). In the fast flow initiation regions of some outlet glaciers (e.g. Petermann and the northern tributaries of NEGIS) these basal units are closely aligned with the basal water predictions.

4.6 Limitations of bed-echo reflectivity variability as a RES technique to detect basal water

We have added an extra paragraph highlighting unaccounted variables/sources of uncertainty to the approach (including ice fabric and rough-surface transmission losses)

Bed-echo reflectivity variability provides a practical way to automate the detection of a subset of basal water with high confidence at the ice-sheet scale. ~~(specifically, finite water bodies with sharp horizontal gradients in water content).~~ In particular, the technique is well-tuned to detect finite water bodies with sharp horizontal gradients in water content. These attributes are thought likely to be common to basal water in the (likely hard-bedded) interior of the ice-sheet. It is, however, important to note that the approach will fail to identify basal water/wet regions with a homogeneous dielectric and reflective character. This includes the centre of large subglacial lakes (based upon the resolution of our method lakes greater than 5 km in horizontal extent) and regions of more uniformly saturated subglacial till. Since all identified subglacial lakes in Greenland are < 5 km in horizontal extent (Palmer et al., 2013; Howat et al., 2015; Palmer et al., 2015; Willis et al., 2015) we believe that the former scenario is likely to be rare. However, extensive regions of saturated till that evade detection are likely to be present, particularly beneath larger outlet glaciers. ~~such as Petermann~~. This

interpretation is supported by comparison with the bed-echo reflectivity/water map of the Petermann catchment in Chu et al. (2018). Specifically, there is a good agreement between the two water maps in the interior/fast flow initiation region, but this study fails to predict the basal water (likely to be wet sediment) in the main trunk of the outlet glacier. Therefore, if focusing on the catchment-scale subglacial hydrology of Greenland outlet glaciers ~~of these regions~~ (or other glaciogically similar regions of Antarctica) a suite of existing RES techniques to detect and characterise basal water (e.g. Peters et al. (2005); Jacobel et al. (2009); Schroeder et al. (2013); Young et al. (2016)) are better suited. Finally, it is important to add that part of the subglacial water budget is likely to comprise groundwater (Siegert et al., 2017), which would be practically undetectable by RES.

As is generally the case in RES analysis, certain simplifications were made in this study when interpreting bed-returned power. Notably, we did not account for: (i) power modulation due to birefringent propagation/ice fabric anisotropy (e.g. Matsuoka et al. (2012c)); (ii) rough surface transmission (e.g. Grima et al. (2014); Schroeder et al. (2016a)); (iii) scattering by near-surface water. The first of these mechanisms could potentially influence power variability near the ice-divides, since abrupt fabric transitions can be present in these regions (Martin et al., 2009; Drews et al., 2012). However, the zoom plots in these regions (e.g. Fig. 7(b,d), Fig. 9(d)) indicate that the water predictions occur over a multiple range of flight-track orientations relative to the ice divide (which should correlate with orientation of the principle dielectric axes). We therefore can discount ice fabric having a dominant influence upon the results. The second and third of these mechanisms will influence power variability primarily in faster flowing regions toward the margins, as these regions have higher surface roughness (e.g. MacGregor et al. (2016)) and surface melt (e.g. van de Wal et al. (2008)). The degree of surface-induced power variability depends upon both the surface permittivity and the roughness regime (relative to the radar wavelength) (Schroeder et al., 2016a). It is, however, important to note that we are likely to get the majority of 'false positives' (elevated power variability due to surface modulation) in regions where the bed is predicted to be thawed with high certainty by MacGregor et al. (2016). In turn, the central results in this study - the 'new' regions of basal water/thaw identified in Fig. 7 - are likely to be largely unaffected by surface modulation.

5 Summary and conclusions

This study placed a spatially comprehensive observational constraint upon the basal water distribution beneath the GrIS and, hence, regions of the bed at or above the PMP of ice. The distribution of basal water is influenced by, and has influence upon, multiple ice-sheet and subglacial properties and processes. Subsequently, with a focus upon ice-sheet scale behaviour, we performed an exploratory comparison with related data sets for the GrIS. This included an up-to-date synthesis for the basal thermal state (MacGregor et al., 2016), three different GHF model distributions (Shapiro and Ritz-

woller, 2004; Fox Maule et al., 2009; Martos et al., In revision), bed topography (Morlighem et al., 2017) and predicted subglacial flow paths, and ice surface speed (Joughin et al., 2010, 2016).

Central to the methods in the study was the use of bed-echo reflectivity variability (rather than bed-echo reflectivity) as a RES diagnostic for basal water. Our use of this diagnostic (a form of edge detector) was motivated by its insensitivity to radar attenuation at the ice-sheet scale, and the pragmatic advantages when performing data combination for multiple RES field campaigns. The reflectivity variability diagnostic is, however, only able to detect wet to dry (or wet to frozen) transitions in bed material and is a sufficient (but not necessary) condition for basal water. It will therefore need to be combined with other information to fully map basal water extent and classify basal water bodies.

There was much agreement between the basal water distribution and the thawed marginal regions predicted by MacGregor et al. (2016). However, we identified regions of basal water/thaw in the interior of the ice sheet that were previously classified as likely to be frozen. The most extensive 'new' region of predicted thaw is a quasi-linear 'corridor' feature which extends from NorthGRIP in the south to Petermann in the north. This feature, and the majority of basal water in the northern interior, spatially correlate with elevated GHF inferred from magnetic data by Martos et al. (In revision).

The comparison with bed topography (Morlighem et al., 2017) and predicted flow paths, demonstrated good overall agreement between the basal water storage locations and the geometric constraints imposed by the hydrological pressure potential. However, many of the basal water predictions in the ice-sheet interior occur where ice surface speed (and hence basal motion) is negligible. One plausible explanation is that much of the interior lies upon a hard and undeformable bed. Future investigation of basal control upon GrIS dynamics, should integrate information about basal water and the basal thermal state with better constraints upon bed lithology and geology.

Appendix A: Cross-over analysis for bed-echo reflectivity variability

To assess the internal consistency of the bed-echo reflectivity variability data, Fig. 3(c), we carried out a cross-over analysis at flight-track intersections (defined, as bin centres separated by < 2.5 km in correspondence with 5 km window size). In this analysis we decomposed the data by the radar system categories in Fig. 1(b), using MCoRDS v2 (the most spatially extensive and recent measurements) as a benchmark. We also discounted adjacent postings from the same flight-track.

The cross-over statistics are shown in Table 2, and demonstrate standard deviations that range from 1.13 dB (MCoRDS v2 - MCoRDS v2) to 1.69 dB (MCoRDS v2 - MCRDS). The relatively high standard deviation for MCoRDS v2 - MCRDS is likely to arise because the MCRDS coverage is almost exclusively in outlet glacier regions where power variability due to surface roughness and crevassing will be higher. There is no significant bias due to radar centre frequency (MCoRDS v2 and MCoRDS are for 195 MHz, whereas MCRDS and ACORDS are for 150 MHz). However, MCoRDS does have a small negative bias. Since the underlying mechanism for this is unclear we do not empirically correct the data. We note that this is a conservative approach (since $\sigma_{[R]}$ is underestimated), and is logically consistent with $\sigma_{[R]}$ being used as a sufficient condition for basal water (i.e. basal water may be present that is not above the prescribed variability threshold).

The cross-over standard deviation values for $\sigma_{[R]}$ in Table 2 should not be interpreted as a standard errors (and are likely significant overestimates) as the flight-track windows do not necessarily sample the same region of the glacier bed. This contrasts with performing cross-over analysis of bed-echo power/reflectivity where the Fresnel zone (length scale $\sim$ 100 m) defines a spatial overlap. As a form of edge detector, the purpose of the $\sigma_{[R]}$ metric is to identify a signal attributable to basal water within a 5 km region (rather than to coarse-grain an average value). Additionally, the along-track data in Fig. 2 shows that $\sigma_{[R]}$ can rapidly fluctuate at a 5 km length scale. We therefore point toward the high degree of spatial structure for $\sigma_{[R]}$ in Fig. 3, and the water predictions in Figs. 7 - 10 as evidence for the robustness of the approach.

Data availability

The CSARP L1B RES data are available from CReSIS at https://data.cresis.ku.edu/data/ rds/ and are documented in Paden (2015). The profile in Fig. 2(a) is from data segment 2012050804 from the 2012 P3 season and the profile in Fig. 2(b) is from data segment 2014051601 from the 2014 P3 season. The Greenland basal thermal state synthesis (MacGregor et al., 2016), ice thickness and topography data sets (BedMachine V3) (Morlighem et al., 2017), and ice surface speed (Joughin et al., 2016), are archived by NSIDC at http://dx.doi.org/10.5067/ R4MWDWWUWQF9, https://nsidc.org/data/idbmg4 and https://nsidc.org/data/NSIDC-0670/versions/1 respectively. The GHF maps by Fox Maule et al. (2009) and Shapiro and Ritzwoller (2004) and available at http://www.dmi.dk/dmi/dkc09-09.pdf and http://ciei.colorado/edu/∼nshapiro/MODEL/ASC_VERSION/index.html respectively.

Pending review, the basal water distribution will be provided as csv files on both a season-by-season basis and for the full (13 season) data set. The data columns will correspond to: (A) latitude, (B) longitude, (C) water binary value, at a 1 km along-track posting. The water binary value will correspond to: 1 $\equiv$ a 5 km bin with water ($\sigma_{[R]}$ > 6 dB, robust to a $\pm$ 20 $\%$ perturbation in $< N >$), 0 $\equiv$ a 5 km bin with a majority of good quality bed-echoes but no water, NaN $\equiv$ a 5 km bin with a majority of poor quality bed-echoes (interpreted as no coverage). A GIS shape file~~geotiff overlay~~ for the water predictions and radar flight-tracks will also be provided.

Author contributions

The study was initiated by JLB and co-advised by MJS as part of the Basal Properties of Greenland Project. TMJ wrote the paper, analysed the radar data, and, with advice from DMS, developed the water detection method. CNW and MAC developed the GIS mapping environment and modelled the subglacial flow paths. JDP and DMS both advised on radar data processing. YMM contributed the new heat flux distribution and advised on the interpretation of the heat flux models. PH contributed the GISM temperature field and advised on ice-sheet thermodynamics. All authors commented on the paper draft and contributed to the interpretation of the science.

Competing interests

JLB is an advisory editor of The Cryosphere. The authors declare that they have no conflict of interests.

Acknowledgments

The project was primarily supported by UK NERC grant NE/M000869/1 as part of the Basal Properties of Greenland project. T.M.J. was also supported by an EU Horizons 2020 grant 747336-

BRISRES-H2020-MSCA-IF-2016. M.A.C. was supported by the UK NERC grant NE/L002434/1 as part of the NERC Great Western Four + (GW4+) Doctoral Training Partnership. D.M.S. was supported by a grant from the NASA Cryospheric Sciences Program. We acknowledge the use of data products from CReSIS generated with support from NASA grant NNX16AH54G. We would like to thank Reinhard Drews and an anonymous reviewer for their thoughtful and constructive comments, and Kenichi Matsuoka for being our review editor. We would also like to thank Winnie Chu, Stanford University, for her helpful discussions.

References

Andersen, K. K., Azuma, N., Barnola, J.-M., Bigler, M., Biscaye, P., Caillon, N., Chappellaz, J., Clausen, H. B., Dahl-Jensen, D., Fischer, H., Flückiger, J., Fritzsche, D., Fujii, Y., Goto-Azuma, K., Grønvold, K., Gundestrup, N. S., Hansson, M., Huber, C., Hvidberg, C. S., Johnsen, S. J., Jonsell, U., Jouzel, J., Kipfstuhl, S., Landais, A., Leuenberger, M., Lorrain, R., Masson-Delmotte, V., Miller, H., Motoyama, H., Narita, H., Popp, T., Rasmussen, S. O., Raynaud, D., Rothlisberger, R., Ruth, U., Samyn, D., Schwander, J., Shoji, H., Siggard-Andersen, M.-L., Steffensen, J. P., Stocker, T., Sveinbjörnsdóttir, A. E., Svensson, A., Takata, M., Tison, J.-L., Thorsteinsson, T., Watanabe, O., Wilhelms, F., and White, J. W. C.: High-resolution record of Northern Hemisphere climate extending into the last interglacial period, Nature, 431, 147–151, doi:10.1038/nature02805, 2004.

Artemieva, I. M.: Global $1^\circ \times 1^\circ$ thermal model TC1 for the continental lithosphere: Implications for lithosphere secular evolution, Tectonophysics, 416, 245–277, doi:10.1016/j.tecto.2005.11.022, 2006.

Bamber, J. L., Griggs, J. A., Hurkmans, R. T. W. L., Dowdeswell, J. A., Gogineni, S. P., Howat, I., Mouginot, J., Paden, J., Palmer, S., Rignot, E., and Steinhage, D.: A new bed elevation dataset for Greenland, The Cryosphere, 7, 499–510, doi:10.5194/tc-7-499-2013, 2013a.

Bamber, J. L., Siegert, M. J., Griggs, J. A., Marshall, S. J., and Spada, G.: Paleofluvial Mega-Canyon Beneath the Central Greenland Ice Sheet, Science, 341, 997–1000, doi:10.1126/science.1239794, 2013b.

Beem, L. H., Cavitte, M. G. P., Blankenship, D. D., Carter, S. P., and Young, D. A.: Ice-flow reorganization within the East Antarctic Ice Sheet deep interior, Geological Society, London, Special Publications, p. SP461.14, doi:10.1144/SP461.14, 2017.

Bell, R. E., Tinto, K., Das, I., Wolovick, M., Chu, W., Creyts, T. T., Frearson, N., Abdi, A., and Paden, J. D.: Deformation, warming and softening of Greenland's ice by refreezing meltwater, Nature Geoscience, 7, 497–502, doi:10.1038/ngeo2179, 2014.

Berry, M. V.: Theory of radio echoes from glacier beds, Journal of Glaciology, 15, 65–74, 1975.

Bogorodsky, V. R., Bentley, C. R., and Gudmandsen, P. E.: Radioglaciology, chap. 6, p. 216, D. Reidel Publishing Company, 1983.

Bons, P. D., Jansen, D., Mundel, F., Bauer, C. C., Binder, T., Eisen, O., Jessell, M. W., Llorens, M. G., Steinbach, F., Steinhage, D., and Weikusat, I.: Converging flow and anisotropy cause large-scale folding in Greenland's ice sheet, 7, 1–6, doi:10.1038/ncomms11427, http://dx.doi.org/10.1038/ncomms11427, 2016.

Buchardt, S. L. and Dahl-Jensen, D.: Estimating the basal melt rate at North GRIP using a Monte Carlo technique, Annals of Glaciology, 45, 137–142, doi:10.3189/172756407782282435, 2007.

Carter, S. P., Blankenship, D. D., Peters, M. E., Young, D. a., Holt, J. W., and Morse, D. L.: Radar-based subglacial lake classification in Antarctica, Geochemistry, Geophysics, Geosystems, 8, n/a–n/a, doi:10.1029/2006GC001408, http://doi.wiley.com/10.1029/2006GC001408, 2007.

Christianson, K., Peters, L. E., Alley, R. B., Anandakrishnan, S., Jacobel, R. W., Riverman, K. L., Muto, A., and Keisling, B. A.: Dilatant till facilitates ice-stream flow in northeast Greenland, Earth and Planetary Science Letters, 401, 57–69, doi:10.1016/j.epsl.2014.05.060, 2014.

Chu, V. W.: Greenland ice sheet hydrology, Progress in Physical Geography, 38, 19–54, doi:10.1177/0309133313507075, 2014.

Chu, W., Schroeder, D. M., Seroussi, H., Creyts, T. T., Palmer, S. J., and Bell, R. E.: Extensive winter subglacial water storage beneath the Greenland Ice Sheet, Geophysical Research Letters, 43, 12,484–12,492, doi:10.1002/2016GL071538, 2016.

Chu, W., Schroeder, D. M., Seroussi, H. S., Creyts, T. T., and Bell, R. E.: Complex basal thermal transition near the onset of Petermann Glacier, Greenland, Journal of Geophysical Research: Earth Surface, 123, 1–11, doi:10.1029/2017JF004561, http://doi.wiley.com/10.1029/2017JF004561, 2018.

Cooper, M. A., Michaelides, K., Siegert, M. J., and Bamber, J. L.: Paleofluvial landscape inheritance for Jakobshavn Isbræ catchment, Greenland, Geophysical Research Letters, 43, 6350–6357, doi:10.1002/2016GL069458, 2016.

Corr, H., Moore, J. C., and Nicholls, K. W.: Radar Absorption due to Impurities in Antarctic Ice, Geophysical Research Letters, 20, 1071–1074, 1993.

Creyts, T. T. and Schoof, C. G.: Drainage through subglacial water sheets, Journal of Geophysical Research: Earth Surface, 114, 1–18, doi:10.1029/2008JF001215, 2009.

Cuffey, K. M., Clow, G. D., Alley, R. B., Stuiver, M., Waddington, E. D., and Saltus, R. W.: Large Arctic Temperature Change at the Wisconsin-Holocene Glacial Transition, 270, 455–458, doi:10.1126/science.270.5235.455, 1995.

Dahl-Jensen, D., Mosegaard, K., Gundestrup, N., Clow, G. D., Johnsen, S. J., Hansen, A. W., and N., B.: Past Temperatures Directly from the Greenland Ice Sheet, Science, 282, 268–271, doi:10.1126/science.282.5387.268, 1998.

Dahl-Jensen, D., Gundestrup, N., Gogineni, S. P., and Miller, H.: Basal melt at NorthGRIP modeled from borehole, ice-core and radio-echo sounder observations, Annals of Glaciology, 37, 207–212, doi:10.3189/172756403781815492, 2003.

Dawes, P. R.: The bedrock geology under the Inland Ice: the next major challenge for Greenland mapping, Geological Survey of Denmark and Greenland Bulletin, 17, 57–60, 2009.

Dow, C. F., Karlsson, N. B., and Werder, M. A.: Limited Impact of Subglacial Supercooling Freeze-on for Greenland Ice Sheet Stratigraphy, Geophysical Research Letters, 45, 1481–1489, doi:10.1002/2017GL076251, 2018.

Drews, R., Eisen, O., Steinhage, D., Weikusat, I., Kipfstuhl, S., and Wilhelms, F.: Potential mechanisms for anisotropy in ice-penetrating radar data, Journal of Glaciology, 58, 613–624, doi:10.3189/2012JoG11J114, 2012.

Fahnestock, M., Abdalati, W., Joughin, I., Brozena, J., and Gogineni, P.: High geothermal heat flow, Basal melt, and the origin of rapid ice flow in central Greenland., Science, 294, 2338–2342, doi:10.1126/science.1065370, 2001.

Forsyth, D. A., Morel-A-L'Huissier, P., Asudeh, I., and Green, A. G.: Alpha Ridge and Iceland - Products of the same plume?, Journal of Geodynamics, 6, 197–214, doi:10.1016/0264-3707(86)90039-6, 1986.

Fox Maule, C., Purucker, M., and Olsen, N.: Inferring magnetic crustal thickness and geothermal heat flux from crustal magnetic fieldmodels: Rep. 09-09, Danish Meteorol. Inst., Copenhagen., http://www.dmi.dk/dmi/dkc09-09.pdf, [last access: Oct 2017], 2009.

Goelzer, H., Huybrechts, P., Fürst, J. J., Nick, F. M., Andersen, M. L., Edwards, T. L., Fettweis, X., Payne, A. J., and Shannon, S.: Sensitivity of Greenland ice sheet projections to model formulations, Journal of Glaciology, 59, 733–749, doi:10.3189/2013JoG12J182, 2013.

Gogineni, S., Yan, J.-B., Paden, J., Leuschen, C., Li, J., Rodriguez-Morales, Braaten, D., Purdon, K., Wang, Z., Liu, W., and Gauch, J.: Bed topography of Jakobshavn Isbrae, Greenland, and Byrd Glacier, Antarctica, Journal of Glaciology, 60, 813–833, doi:10.3189/2014JoG14J129, 2014.

Greve, R.: Relation of measured basal temperatures and the spatial distribution of the geothermal heat flux for the Greenland ice sheet, Annals of Glaciology, 42, 424–432, doi:10.3189/172756405781812510, 2005.

Grima, C., Schroeder, D. M., Blankenship, D. D., and Young, D. A.: Planetary landing-zone reconnaissance using ice-penetrating radar data: Concept validation in Antarctica, Planetary and Space Science, 103, 191–204, doi:10.1016/j.pss.2014.07.018, 2014.

Gundestrup, N. S. and Hansen, L. H.: Bore-hole survey at Dye 3, South Greenland, Journal of Glaciology, 30, 1984.

Henriksen, N.: Geological History of Greenland. Four Billion Years of Earths Evolution, vol. 1st edition, Geological Survery of Greenland and Denmark, (GEUS), 2008.

Howat, I. M., Porter, C., Noh, M. J., Smith, B. E., and Jeong, S.: Brief communication: Sudden drainage of a subglacial lake beneath the Greenland Ice Sheet, Cryosphere, 9, 103–108, doi:10.5194/tc-9-103-2015, 2015.

Huybrechts, P.: Basal temperature conditions of the Greenland ice sheet during the glacial cycles, Annals of Glaciology, 23, 877–887, 1996.

Jacobel, R. W., Welch, B. C., Osterhouse, D., Pettersson, R., and MacGregor, J. A. M.: Spatial variation of radar-derived basal conditions on Kamb Ice Stream, West Antarctica, Annals of Glaciology, 50, 10–16, 2009.

Jordan, T. M., Bamber, J. L., Williams, C. N., Paden, J. D., Siegert, M. J., Huybrechts, P., Gagliardini, O., and Gillet-Chaulet, F.: An ice-sheet-wide framework for englacial attenuation from ice-penetrating radar data, The Cryosphere, 10, 1547–1570, doi:10.5194/tc-10-1547-2016, 2016.

Jordan, T. M., Cooper, M. A., Schroeder, D. M., Williams, C. N., Paden, J. D., Siegert, M. J., and Bamber, J. L.: Self-affine subglacial roughness: Consequences for radar scattering and basal water discrimination in northern Greenland, The Cryosphere, 11, 1247–1264, doi:10.5194/tc-11-1247-2017, 2017.

Joughin, I., Smith, B. E., Howat, I. M., Scambos, T., and Moon, T.: Greenland flow variability from ice-sheet-wide velocity mapping, Journal of Glaciology, 56, 415–430, doi:10.3189/002214310792447734, 2010.

Joughin, I., Smith, B., Howat, I., and Scambos, T.: Multi-year Greenland Ice Sheet Velocity Mosaic, Version 1., http://nsidc.org/data/NSIDC-0670/versions/1, [last access: Oct 2017], 2016.

Layberry, R. L. and Bamber, J. L.: A new ice thickness and bed data set for the Greenland ice sheet 2. Relationship between dynamics and basal topography, Journal of Geophysical Research, 106, 33 781–33 788, 2001.

Le Brocq, A. M., Payne, A. J., Siegert, M. J., and Alley, R. B.: A subglacial water flow model for West Antarctica, J. Glaciol., 55, 879–888, doi:10.3189/002214309790152564, 2009.

Livingstone, S. J., Chu, W., Ely, J. C., and Kingslake, J.: Paleofluvial and subglacial channel networks beneath Humboldt Glacier, Greenland, Geology, 45, 551–554, doi:10.1130/G38860.1, 2017.

MacGregor, J. A., Winebrenner, D. P., Conway, H., Matsuoka, K., Mayewski, P. A., and Clow, G. D.: Modeling englacial radar attenuation at Siple Dome, West Antarctica, using ice chemistry and temperature data, Journal of Geophysical Research, 112, F03 008, doi:10.1029/2006JF000717, 2007.

MacGregor, J. A., Matsuoka, K., Waddington, E. D., Winebrenner, D. P., and Pattyn, F.: Spatial variation of englacial radar attenuation: Modeling approach and application to the Vostok flowline, Journal of Geophysical Research, 117, F03 022, doi:10.1029/2011JF002327, 2012.

MacGregor, J. A., Catania, G. A., Conway, H., Schroeder, D. M., Joughin, I., Young, D. A., Kempf, S. D., and Blankenship, D. D.: Weak bed control of the eastern shear margin of Thwaites Glacier, West Antarctica, Journal of Glaciology, 59, 900–912, doi:10.3189/2013JoG13J050, 2013.

MacGregor, J. A., Fahnestock, M. A., Catania, G. A., Paden, J. D., Gogineni, S. P., Young, S. K., Rybarski, S. C., Mabrey, A. N., Wagman, B. M., and Morlighem, M.: Radiostratigraphy and age structure of the Greenland Ice Sheet, pp. 1–30, doi:10.1002/2014JF003215.Received, 2015a.

MacGregor, J. A., Li, J., Paden, J. D., Catania, G. A., Clow, G. D., Fahnestock, M. A., Gogineni, S. P., Grimm, R. E., Morlighem, M., Nandi, S., Seroussi, H., and Stillman, D. E.: Radar attenuation and temperature within the Greenland Ice Sheet, Journal of Geophysical Research: Earth Surface, 120, 983–1008, doi:10.1002/2014JF003418, 2015b.

MacGregor, J. A., Fahnestock, M. A., Catania, G. A., Aschwanden, A., Clow, G. D., Colgan, W. T., Gogineni, S. P., Morlighem, M., Nowicki, S. M. J., Paden, J. D., Price, S. F., and Seroussi, H.: A synthesis of the basal thermal state of the Greenland ice sheet, Journal of Geophysical Research: Earth Surface, 127, 1328–1350, doi:10.1002/2015JF003803, 2016.

Martin, C., Gudmundsson, G. H., Pritchard, H. D., and Gagliardini, O.: On the effects of anisotropic rheology on ice flow, internal structure, and the age-depth relationship at ice divides, Journal of Geophysical Research: Earth Surface, 114, 1–18, doi:10.1029/2008JF001204, 2009.

Martinez, A., Byrnes, A. P., Survey, K. G., and Avenue, C.: Modeling Dielectric-constant Values of Geologic Materials: An Aid to Ground-Penetrating Radar Data Collection and Interpretation, Current Research in Earth Sciences, Kansas Geological Survey Bulletin, 247, 1–16, doi:10.1.1.22.9348, 2001.

Martos, Y. M., Catalan, M., Jordan, T. A., Golynsky, A., Golynsky, D., Eagles, G., and Vaughan, D. G.: Heat flux distribution of Antarctica unveiled, Geophysical Research Letters, doi:10.1002/2017GL075609, http://doi.wiley.com/10.1002/2017GL075609, 2017.

Martos, Y. M., Jordan, T. A., Catalan, M., Jordan, T. M., Bamber, J. L., and Vaughan, D.: Geothermal heat flux reveals the Iceland hotspot track underneath Greenland, In revision.

Matsuoka, K.: Pitfalls in radar diagnosis of ice-sheet bed conditions: Lessons from englacial attenuation models, Geophysical Research Letters, 38, 1–5, doi:10.1029/2010GL046205, 2011.

Matsuoka, K., MacGregor, J. A., and Pattyn, F.: Using englacial radar attenuation to better diagnose the subglacial environment: A review, Proceedings of the 13th International Conference on Ground Penetrating Radar, GPR 2010, doi:10.1109/ICGPR.2010.5550161, 2010.

Matsuoka, K., MacGregor, J. A., and Pattyn, F.: Predicting radar attenuation within the Antarctic ice sheet, Earth and Planetary Science Letters, 359-360, 173–183, doi:10.1016/j.epsl.2012.10.018, 2012a.

Matsuoka, K., Pattyn, F., Callens, D., and Conway, H.: Radar characterization of the basal interface across the grounding zone of an ice-rise promontory in East Antarctica, Annals of Glaciology, 53, 29–34, doi:10.3189/2012AoG60A106, 2012b.

Matsuoka, K., Power, D., Fujita, S., and Raymond, C. F.: Rapid development of anisotropic ice-crystal-alignment fabrics inferred from englacial radar polarimetry, central West Antarctica, Journal of Geophysical Research: Earth Surface, 117, 1–16, doi:10.1029/2012JF002440, 2012c.

Moon, T., Joughin, I., Smith, B., Van Den Broeke, M. R., Van De Berg, W. J., Noël, B., and Usher, M.: Distinct patterns of seasonal Greenland glacier velocity, Geophysical Research Letters, 41, 7209–7216, doi:10.1002/2014GL061836, 2014.

Morlighem, M., Williams, C. N., Rignot, E., An, L., Arndt, J. E., Bamber, J. L., Catania, G., Chauché, N., Dowdeswell, J. A., Dorschel, B., Fenty, I., Hogan, K., Howat, I., Hubbard, A., Jakobsson, M., Jordan, T. M., Kjeldsen, K. K., Millan, R., Mayer, L., Mouginot, J., Noël, B. P. Y., O'Cofaigh, C., Palmer, S., Rysgaard, S., Seroussi, H., Siegert, M. J., Slabon, P., Straneo, F., van den Broeke, M. R., Weinrebe, W., Wood, M., and Zinglersen, K. B.: BedMachine v3: Complete Bed Topography and Ocean Bathymetry Mapping of Greenland From Multibeam Echo Sounding Combined With Mass Conservation, Geophysical Research Letters, 44, 11,051–11,061, doi:10.1002/2017GL074954, 2017.

Murray, A. E., Kenig, F., Fritsen, C. H., Mckay, C. P., Cawley, K. M., Edwards, R., Kuhn, E., Mcknight, D. M., Ostrom, N. E., Peng, V., Ponce, A., Priscu, J. C., Samarkin, V., Townsend, A. T., Wagh, P., Young, S. A., To, P., and Doran, P. T.: Microbial life at -13°C in the brine of an ice-sealed Antarctic lake, Proceedings of the National Academy of Sciences, 109, 2–7, doi:10.1073/pnas.1208607109, 2012.

Neal, C. S.: Radio echo determination of basal roughness characteristics on the Ross Ice Shelf, Ann. Glaciol., 3, 216– 221, 1982.

Oswald, G. and Gogineni, S.: Recovery of subglacial water extent from Greenland radar survey data, Journal of Glaciology, 54, 94–106, doi:10.3189/002214308784409107, 2008.

Oswald, G. K. A. and Gogineni, S. P.: Mapping Basal Melt Under the Northern Greenland Ice Sheet, IEEE Transactions on Geoscience and Remote Sensing, 50, 585–592, doi:10.1109/TGRS.2011.2162072, 2012.

Paden, J.: Radar Depth Sounder, Centre for Remote Sensings of Ice Sheets, http://data.cresis.ku.edu/data/rds/rds_readme.pdf, [last access: Dec 2015], 2015.

Palmer, S., McMillan, M., and Morlighem, M.: Subglacial lake drainage detected beneath the Greenland ice sheet, Nature Communications, 6, 8408, doi:10.1038/ncomms9408, 2015.

Palmer, S. J., Dowdeswell, J. A., Christoffersen, P., Young, D. A., Blankenship, D. D., Greenbaum, J. S., Benham, T., Bamber, J., and Siegert, M. J.: Greenland subglacial lakes detected by radar, Geophysical Research Letters, 40, 6154–6159, doi:10.1002/2013GL058383, 2013.

Peters, M. E., Blankenship, D. D., and Morse, D. L.: Analysis techniques for coherent airborne radar sounding: Application to West Antarctic ice streams, Journal of Geophysical Research, 110, B06 303, doi:10.1029/2004JB003222, 2005.

Pollack, H. N., Hurter, S. J., and Johnson, J. R.: Heat flow from the Earth's interior: Analysis of the global data set, Reviews of Geophysics, 31, 267–280, doi:10.1029/93RG01249, 1993.

Rennermalm, A. K., Moustafa, S. E., Mioduszewski, J., Chu, V. W., Forster, R. R., Hagedorn, B., Harper, J. T., Mote, T. L., Robinson, D. A., Shuman, C. A., Smith, L. C., and Tedesco, M.: Understanding Greenland

ice sheet hydrology using an integrated multi-scale approach, Environmental Research Letters, 8, 015 017, doi:10.1088/1748-9326/8/1/015017, 2013.

Rezvanbehbahani, S., Stearns, L. A., Kadivar, A., Walker, J. D., and van der Veen, C. J.: Predicting the geothermal heat flux in Greenland: a Machine Learning approach, Geophysical Research Letters, doi:10.1002/2017GL075661, 2017.

Rippin, D. M.: Bed roughness beneath the Greenland ice sheet, Journal of Glaciology, 59, 724–732, doi:10.3189/2013JoG12J212, 2013.

Rodriguez-Morales, F., Gogineni, S., Leuschen, C. J., Paden, J. D., Li, J., Lewis, C. C., Panzer, B., Gomez-Garcia Alvestegui, D., Patel, A., Byers, K., Crowe, R., Player, K., Hale, R. D., Arnold, E. J., Smith, L., Gifford, C. M., Braaten, D., and Panton, C.: Advanced multifrequency radar instrumentation for polar Research, IEEE Transactions on Geoscience and Remote Sensing, 52, 2824–2842, doi:10.1109/TGRS.2013.2266415, 2014.

Rogozhina, I., Hagedoorn, J. M., Martinec, Z., Fleming, K., Soucek, O., Greve, R., and Thomas, M.: Effects of uncertainties in the geothermal heat flux distribution on the Greenland Ice Sheet: An assessment of existing heat flow models, Journal of Geophysical Research, 117, 1–16, doi:10.1029/2011JF002098, 2012.

Rogozhina, I., Petrunin, A. G., Vaughan, A. P. M., Steinberger, B., Johnson, J. V., Kaban, M. K., Calov, R., Rickers, F., Thomas, M., and Koulakov, I.: Melting at the base of the Greenland ice sheet explained by Iceland hotspot history, Nature Geoscience, 9, 366–369, doi:10.1038/ngeo2689, 2016.

Rutishauser, A., Blankenship, D. D., Sharp, M., Skidmore, M. L., Greenbaum, J. S., Grima, C., Schroeder, D. M., Dowdeswell, J. A., and Young, D. A.: Discovery of a hypersaline subglacial lake complex beneath Devon Ice Cap, Canadian Arctic, Science Advances, 4, eaar4353, doi:10.1126/sciadv.aar4353, http://advances.sciencemag.org/lookup/doi/10.1126/sciadv.aar4353, 2018.

Schoof, C.: Ice-sheet acceleration driven by melt supply variability, Nature, 468, 803–806, doi:10.1038/nature09618, 2010.

Schroeder, D. M., Blankenship, D. D., and Young, D. A.: Evidence for a water system transition beneath Thwaites Glacier, West Antarctica., Proceedings of the National Academy of Sciences of the United States of America, 110, 12 225–8, doi:10.1073/pnas.1302828110, 2013.

Schroeder, D. M., Blankenship, D. D., Young, D. A., and Quartini, E.: Evidence for elevated and spatially variable geothermal flux beneath the West Antarctic Ice Sheet, Proceedings of the National Academy of Sciences, 111, 9070–9072, doi:10.1073/pnas.1405184111, http://www.pnas.org/cgi/doi/10.1073/pnas.1405184111, 2014.

Schroeder, D. M., Grima, C., and Blankenship, D. D.: Evidence for variable grounding-zone and shear-margin basal conditions across Thwaites Glacier, West Antarctica, Geophysics, 81, WA35–WA43, doi:10.1190/geo2015-0122.1, 2016a.

Schroeder, D. M., Seroussi, H., Chu, W., and Young, D. A.: Adaptively constraining radar attenuation and temperature across the Thwaites Glacier catchment using bed echoes, Journal of Glaciology, 62, 1075–1082, doi:10.1017/jog.2016.100, 2016b.

Seroussi, H., Morlighem, M., Rignot, E., Khazendar, A., Larour, E., and Mouginot, J.: Dependence of century-scale projections of the Greenland ice sheet on its thermal regime, Journal of Glaciology, 59, 1024–1034, doi:10.3189/2013JoG13J054, 2013.

Shannon, S. R., Payne, A. J., Bartholomew, I. D., van den Broeke, M. R., Edwards, T. L., Fettweis, X., Gagliardini, O., Gillet-Chaulet, F., Goelzer, H., Hoffman, M. J., Huybrechts, P., Mair, D. W. F., Nienow, P. W., Perego, M., Price, S. F., Smeets, C. J. P. P., Sole, A. J., van de Wal, R. S. W., and Zwinger, T.: Enhanced basal lubrication and the contribution of the Greenland ice sheet to future sea-level rise., Proceedings of the National Academy of Sciences of the United States of America, 110, 14 156–61, doi:10.1073/pnas.1212647110, 2013.

Shapiro, N. M. and Ritzwoller, M. H.: Inferring surface heat flux distributions guided by a global seismic model: Particular application to Antarctica, Earth and Planetary Science Letters, 223, 213–224, doi:10.1016/j.epsl.2004.04.011, 2004.

Shepard, M. K., Campbell, B. A., Bulmber, M. H., Farr, T. G., Gaddis, L. R., and Plaut, J. J.: The roughness of natural terrain: A planetary and remote sensing perspective, Journal of Geophysical Research, 106, 32 777–32 795, doi:10.1029/2000JE001429, 2001.

Shreve, R. L.: Movement of water in glaciers, Journal of Glaciology, 11, 205–214, 1972.

Siegert, M. and Dowdeswell, J. A.: Spatial variations in heat at the base of the Antarctic Ice Sheet from analysis of the thermal regime above subglacial lakes, Journal of Glaciology, 42, 501–509, 1996.

Siegert, M. J., Ross, N., and Le Brocq, A. M.: Recent advances in understanding Antarctic subglacial lakes and hydrology, Philosophical Transactions of the Royal Society A: Mathematical, Physical and Engineering Sciences, 374, 20140 306, doi:10.1098/rsta.2014.0306, 2016.

Siegert, M. J., Kulessa, B., Bougamont, M., Christoffersen, P., Key, K., Andersen, K. R., Booth, A. D., and Smith, A. M.: Antarctic subglacial groundwater: a concept paper on its measurement and potential influence on ice flow, Geological Society, London, Special Publications, 461, SP461.8, doi:10.1144/SP461.8, 2017.

Tedstone, A. J., Nienow, P. W., Sole, A. J., Mair, D. W. F., Cowton, T. R., Bartholomew, I. D., and King, M. A.: Greenland ice sheet motion insensitive to exceptional meltwater forcing, Proceedings of the National Academy of Sciences, 110, 19 719–19 724, doi:10.1073/pnas.1315843110, 2013.

van de Wal, R. S. W., Boot, W., van den Broeke, M. R., Smeets, C., Reijmer, C. H., Donker, J. J. A., and Oerlemans, J.: Large and rapid melt-induced velocity changes in the ablation zone of the Greenland Ice Sheet, Science, 321, 111–113, doi:10.1126/science.1158540, 2008.

van der Veen, C. J.: Fundamentals of Glacier Dynamics, chap. 6, Taylor and Francis, 2 edn., 2013.

Wang, L. and Li, H.: An efficient method for identifying and filling surface depressions in digital elevation models for hydrologic analysis and modelling, International Journal of Geographical Information Science, 20, 193–213, 2006.

Weertman, J.: Comparison between measured and theoretical temperature profiles of the Camp Century, Greenland, Borehole, Journal of Geophysical Research, 73, 2691–2700, 1968.

Willis, M. J., Herried, B. G., Bevis, M. G., and Bell, R. E.: Recharge of a subglacial lake by surface meltwater in northeast Greenland, Nature, 518, 223–227, doi:10.1038/nature14116, 2015.

Wolff, E. W., Miners, W. D., Moore, J. C., and Paren, J. G.: Factors Controlling the Electrical Conductivity of Ice from the Polar Regions: A Summary, Journal of Physics Chemistry B, 5647, 6090–6094, doi:10.1021/jp9631543, 1997.

Wolovick, M. J., Bell, R. E., Creyts, T. T., and Frearson, N.: Identification and control of subglacial water networks under Dome A, Antarctica, Journal of Geophysical Research, 118, 140–154, doi:10.1029/2012JF002555, 2013.

Wolovick, M. J., Creyts, T. T., Buck, W. R., and Bell, R. E.: Traveling slippery patches produce thickness-scale folds in ice sheets, Geophysical Research Letters, 41, 8895–8901, doi:10.1002/2014GL062248, 2014.

Young, D. A., Schroeder, D. M., Blankenship, D. D., Kempf, S. D., and Quartini, E.: The distribution of basal water between Antarctic subglacial lakes from radar sounding, Phil. Trans. R. Soc. A., 374, doi:10.1098/rsta.2014.0297, 2016.

Zwally, H. J., Mario, B. G., Matthew, A. B., and Saba, J. L.: Antarctic and Greenland Drainage Systems, NASA Cryospheric Data, http://icesat4.gsfc.nasa.gov/cryo_data/ant_grn_drainage_systems.php, [last access: Nov 2015], 2012.

Table 1. Dielectric and reflective properties of subglacial materials based upon a compilation of past values by Bogorodsky et al. (1983); Martinez et al. (2001); Peters et al. (2005). The bulk values take into account typical ranges of saturation and porosity for the dielectric mixing of water and ice with the background material. The relative dielectric permittivity of ice is 3.15, which means that 'dry' (just the background dielectric) or 'frozen' (a mixture of the background dielectric with ice) produce a similar range for $[R]$.

Bed material	Relative dielectric permittivity, ϵ	Reflectivity, $[R]$ (dB)
Ground water	80	-2
Wet till	10 to 30	-11 to -6
Wet sandstone	5 to 10	-19 to -11
Dry/frozen granite	5	-19
Dry/frozen limestone	4 to 7	-26 to -14
Dry/frozen till	2 to 6	negligible to -19
Dry/frozen sandstone	2 to 3	-37 to -16

Table 2. Cross-over statistics for $\sigma_{[R]}$ for the different radar instrument classes in Fig. 1(b).

Data comparison	Mean (dB)	SD (dB)
MCoRDs v2 - MCoRDs v2	N/A	1.13
MCoRDs - MCoRDs v2	-0.43	1.18
MCRDS - MCoRDs v2	-0.07	1.69
ACORDS - MCoRDs v2	0.00	1.24

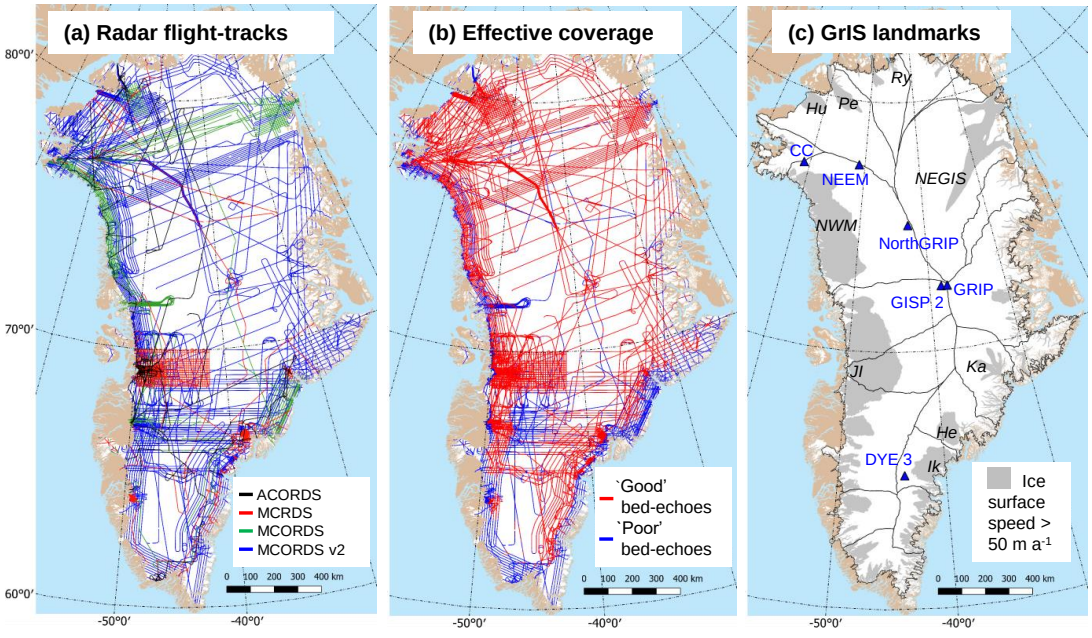

Figure 1. (a) Ice-penetrating radar flight-tracks for different CReSIS radar systems. (b) Effective coverage for 'good quality' radar bed-echoes (corresponding to peak power 10 dB above noise floor). (c) Summary of key GrIS landmarks: temperature boreholes, major drainage basin boundaries (Zwally et al., 2012), and major regions of fast flow identified from ice surface speed (Joughin et al., 2010, 2016). Abbreviations in (c) correspond to: Camp Century (CC), Humboldt (*Hu*), Petermann (*Pe*), Ryder (*Ry*), North East Greenland Ice Stream (*NEGIS*), northwestern margins (*NWM*), Jakobshavn Isbrae (*JI*), Kangerlussuaq (*Ka*), Helheim (*He*) and Ikertivaq (*Ik*). The projection is a Polar Stereographic North (70°N, 45°W) and is used in all future plots.

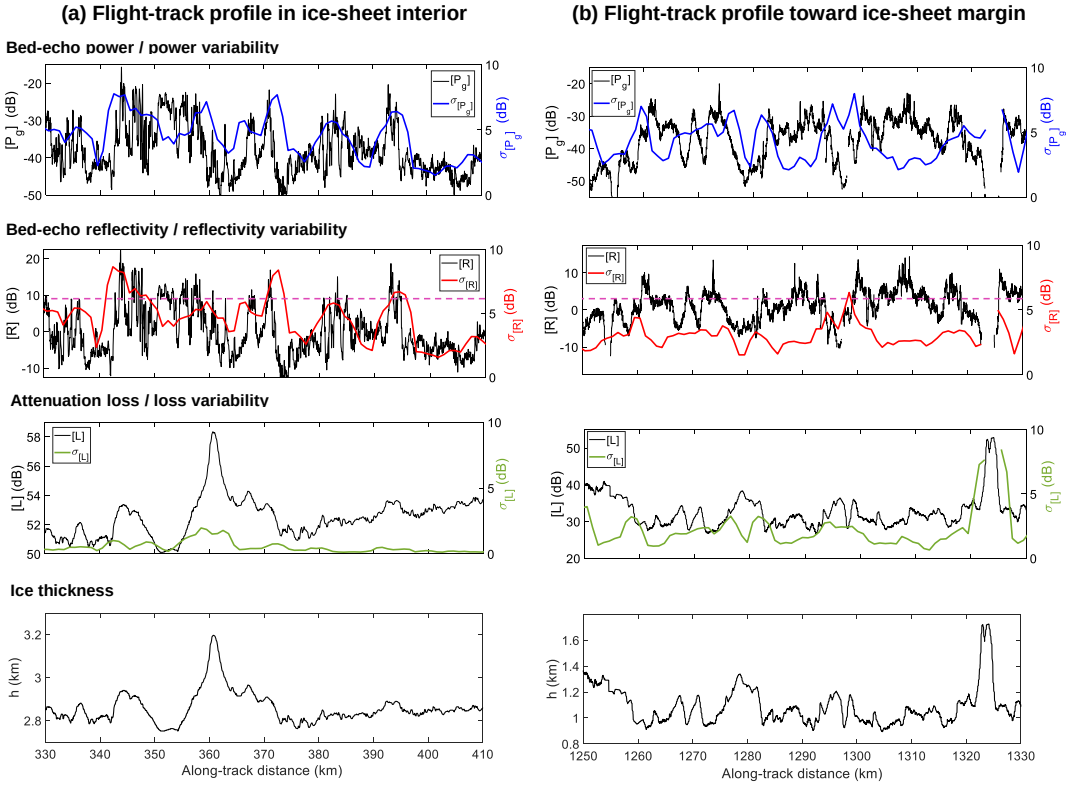

Figure 2. Example flight-track profiles for: bed-echo power and variability, $[P_g]$ and $\sigma_{[P_g]}$, bed-echo reflectivity and variability, $[R]$ and $\sigma_{[R]}$, attenuation loss and variability, $[L]$, $\sigma_{[L]}$, ice thickness, h. Example (a), left of figure, is from the north-central interior of the ice sheet and (b), right of figure, is from the northwestern margins (locations both shown in Fig. 3). The threshold that is later used for water detection, $\sigma_{[R]} > 6$ dB, is indicated by the dashed pink line and values for $[R]$ are relative with zero mean. The variability measures are all calculated at a 5 km length scale with 1 km posting.

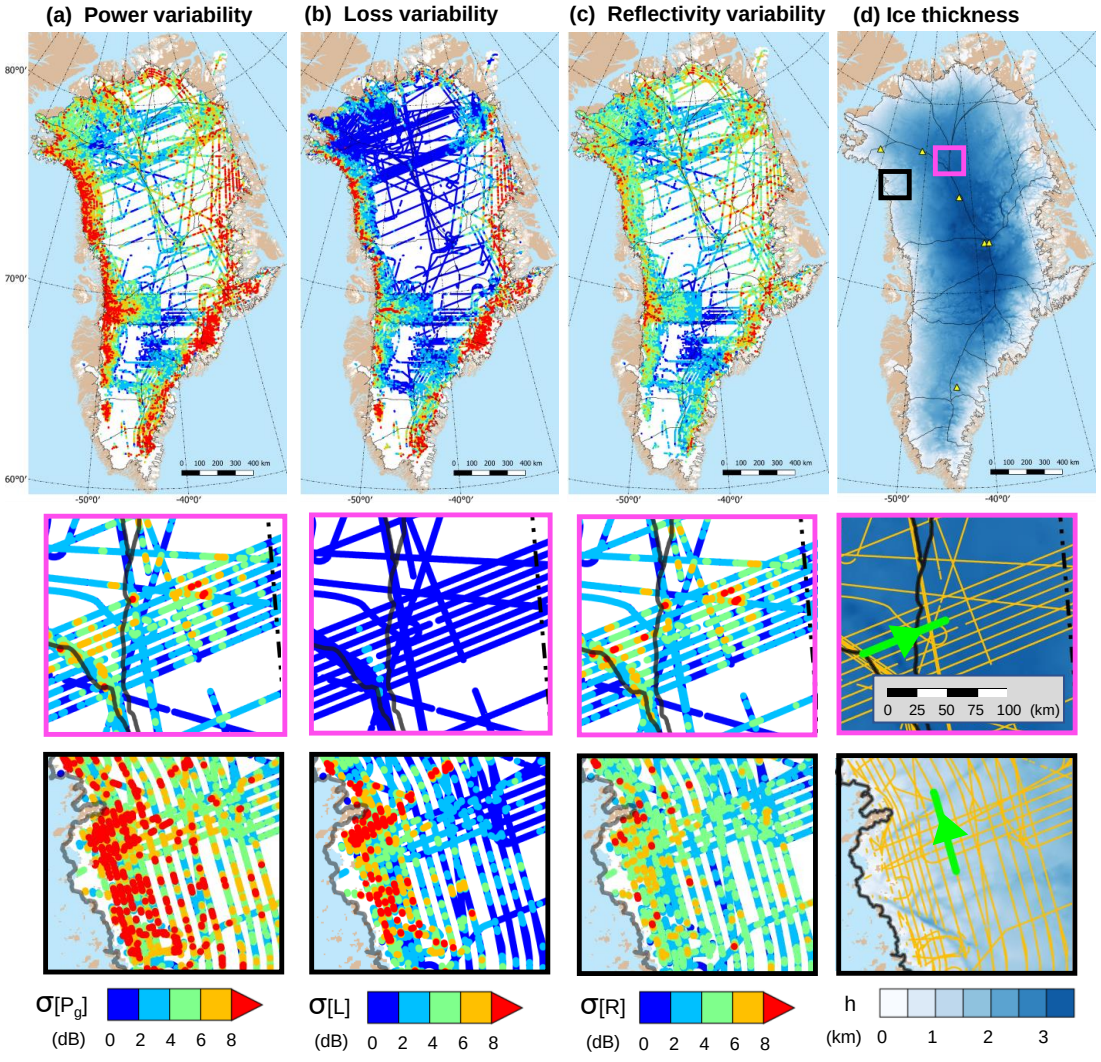

Figure 3. Spatial distributions for: (a) bed-echo power variability $\sigma_{[P_g]}$, (b) attenuation loss variability $\sigma_{[L]}$, (c) bed-echo reflectivity variability $\sigma_{[R]}$, (d) ice thickness, h. Zoom plots with flight-track data at true buffer size (5 km) are shown for the north-central ice sheet (pink bounding box, containing profile in Fig. 2(a)) and northwestern margins (black bounding box, containing profile in Fig. 2(b)). The profiles are indicated in bold green in the ice thickness zoom plots. In plots (a)-(c) higher variability data is stacked on top of lower variability data, which acts to emphasise higher variability. The zoom plots are all have the same scale ($\times$ 8 the resolution of the ice-sheet scale plots).

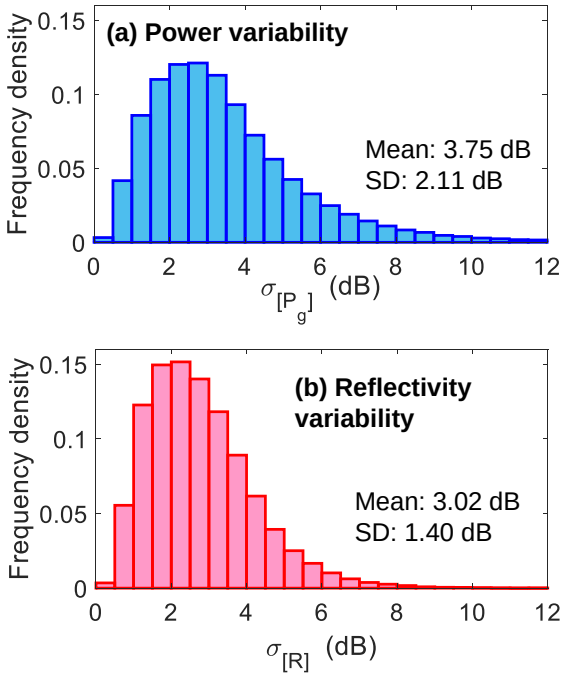

Figure 4. Frequency distributions for: (a) bed-echo power variability, $\sigma_{[P_g]}$ (corresponding to Fig. 3(a)); (b) bed-echo reflectivity variability, $\sigma_{[R]}$ (corresponding to Fig. 3(c)). Later in the study $\sigma_{[R]} > 6$ dB used as threshold criteria for diagnosing the presence of basal water.

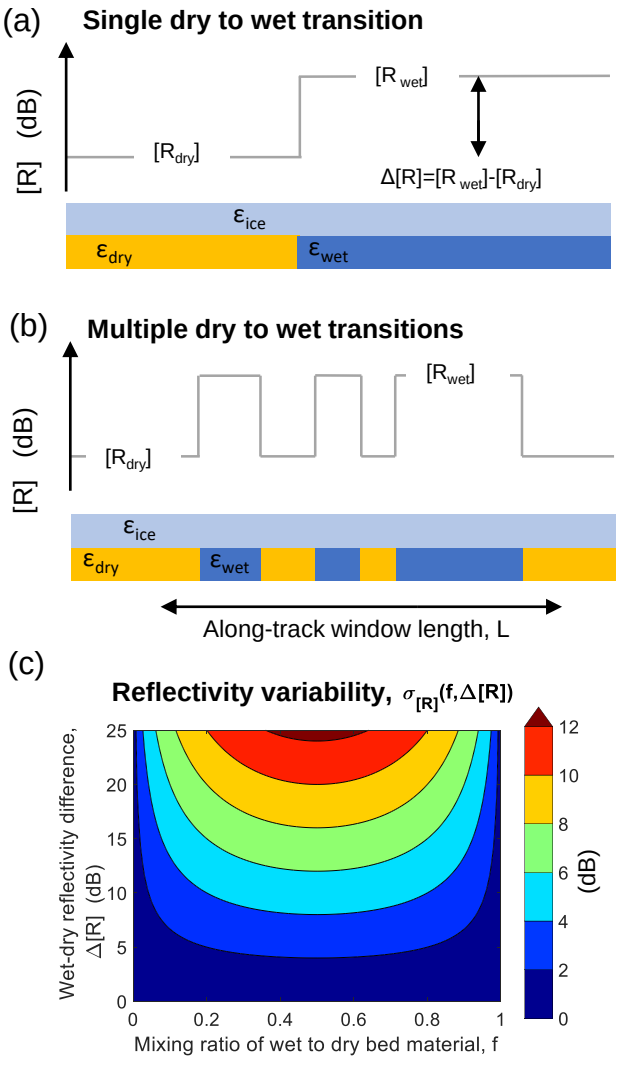

Figure 5. Interpretation of bed-echo reflectivity variability, $\sigma_{[R]}$, as a diagnostic for basal water. (a,b) Schematics of the two-state dielectric model for single and multiple along-track transitions in dry to wet bed material. Both scenarios are identically parameterised by the wet-dry mixing ratio f (visually, the fraction of blue to yellow) and wet-dry reflectivity difference, $\Delta[R] = [R_{wet}] - [R_{dry}]$. (c) Phase-space plot for $\sigma_{[R]}$ as function of f and $\Delta[R]$. $\sigma_{[R]} > 6$ dB is used as a threshold for positive discrimination of basal water (corresponding to green, red and yellow regions).

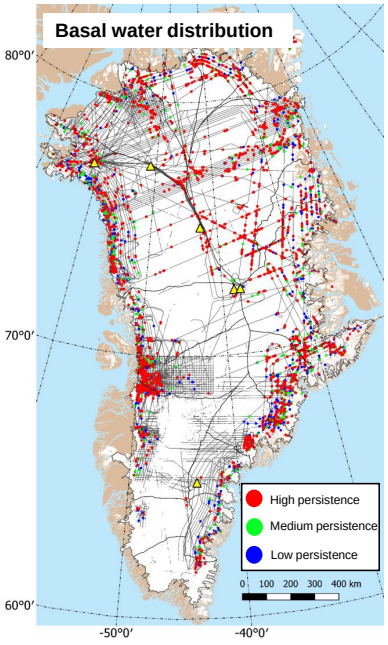

Figure 6. Basal water distribution and robustness to perturbations in the attenuation rate estimate, $< N >$. The original predictions ($\sigma_{[R]}$ > 6 dB) are represented by all three colours.'Persistent' water predictions ($\sigma_{[R]}$ > 6 dB for $\pm$ 20 % and $\pm$ 50 % perturbations to $< N >$) are indicated by the subset of green and red points, and the subset of red points respectively. The subset of red and green points is used in the rest of the paper.

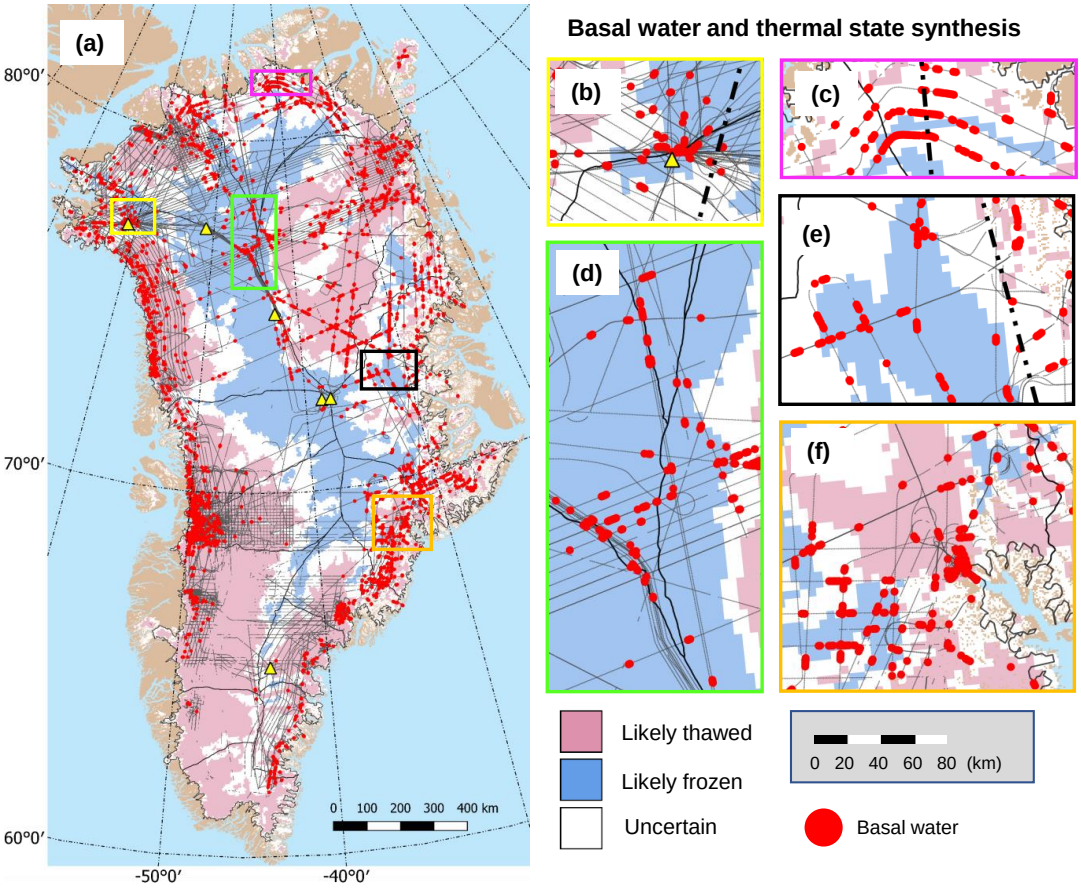

Figure 7. Comparison between basal water distribution and basal thermal state synthesis by MacGregor et al. (2016). (a) Ice-sheet scale. Major regions of disagreement (water in likely frozen regions) are highlighted in the zoom plots. (b) Camp Century. (c) Far north. (d) North-central ice sheet. (e) East of GRIP. (f) Around Kangerlussuaq. The zoom plots all have the same scale ($\times$ 5 the resolution of (a)).

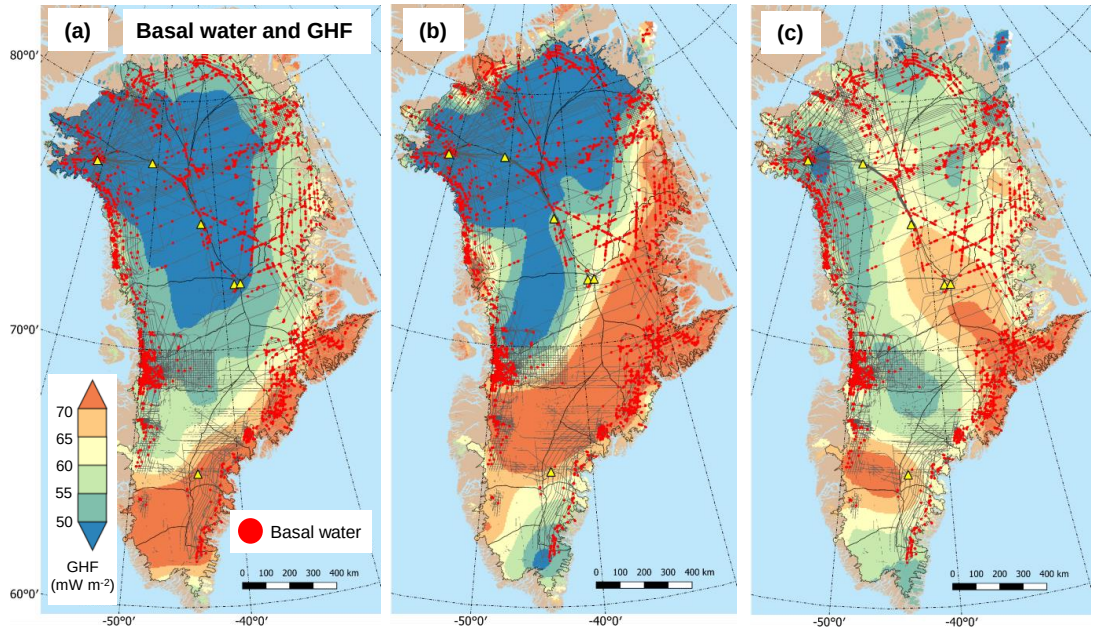

Figure 8. Comparison between basal water distribution and geothermal heat flux (GHF) models. (a) Seismic GHF model by Shapiro and Ritzwoller (2004). (b) Magnetic GHF model by Fox Maule et al. (2009) using satellite data. (c) Magnetic GHF model by Martos et al. (In revision) derived from spectral methods using airborne data. The colour bar scale is the same in all plots and is truncated to emphasise the spatial variation in plot (c).

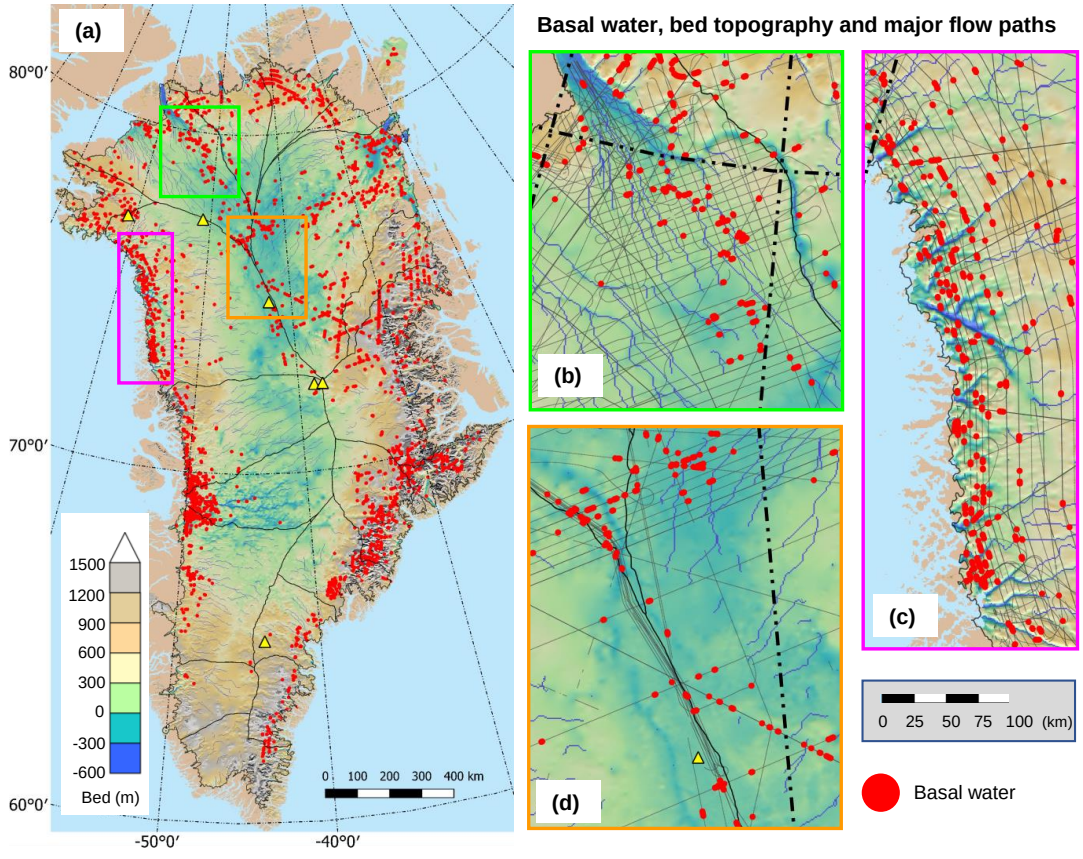

Figure 9. Comparison between basal water distribution, bed topography (Morlighem et al., 2017), and major subglacial flow paths (blue lines). (a) Ice-sheet scale. (b) Petermann catchment. (c) Northwestern margins. (d) North-central ice sheet. To improve clarity the radar flight-tracks are removed from (a) and a hillshade is applied to the bed topography. The zoom plots are all have the same scale ($\times$ 4 the resolution of (a)).

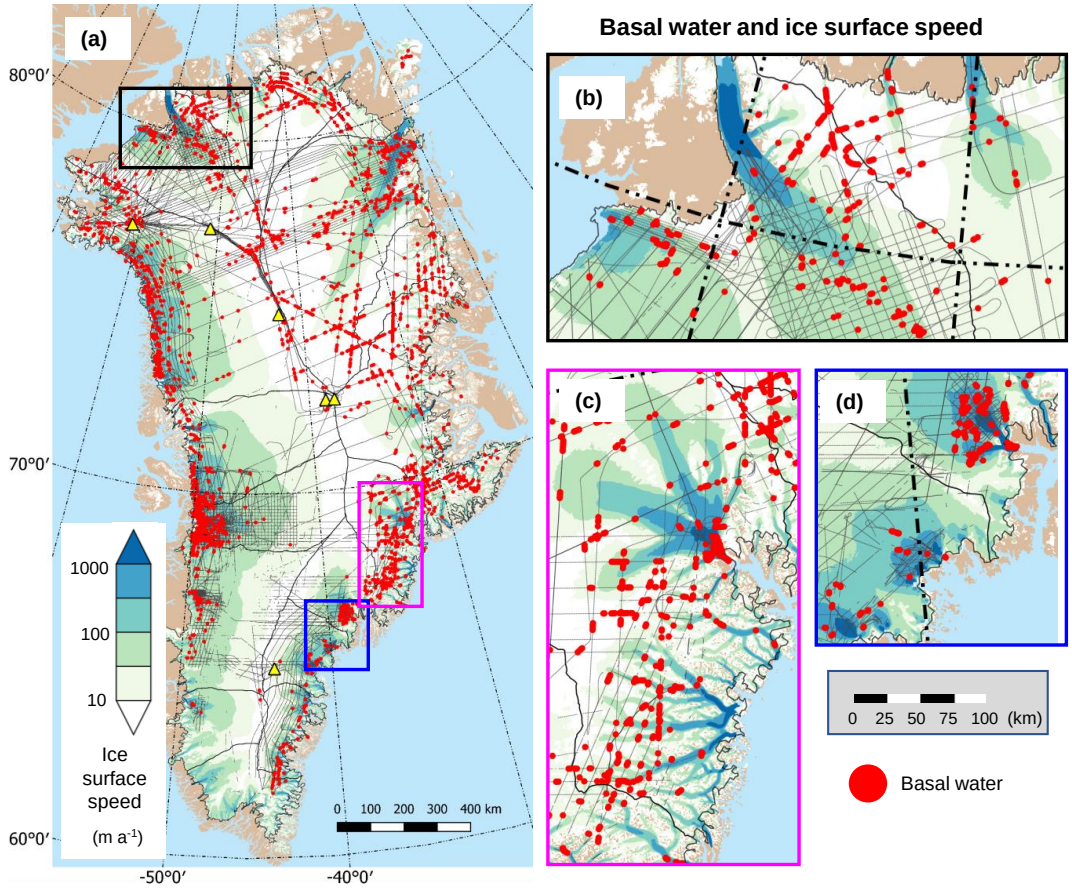

Figure 10. Comparison between basal water distribution and ice surface speed (Joughin et al., 2010, 2016) (logarithmic-scale). (a) Ice-sheet scale. (b) Humboldt, Petermann and Ryder. (c) Kangerlussuaq and region to south. (d) Helheim (north of plot) and Ikertivaq (southwest of plot). The zoom plots are all have the same scale ($\times$ 4 the resolution of (a).)